Polytehnic University of Bucharest

Doctoral School of Materials Science and Engineering

PhD THESIS SUMMARY

CONTRIBUTIONS REGARDING THERMO-MECHANICAL PROCESSING TECHNOLOGIES AND PLASMA JET COATINGS OF CAR BODY ELEMENTS

PhD student: Ing. Năvodariu Nicolae

Scientific coordinator: Prof.habil.dr.ing. Iulian Vasile ANTONIAC

Bucharest

2021

Thanks

At the end of this important phase of my life, I would like to express a few words of thanks to those who have guided me and given me support during my doctoral thesis.

Cordial thanks and great gratitude to my Doctoral leader, Prof.univ.habil.dr.ing. Vasile Iulian Antoniac, from the Polytechnic University of Bucharest, for competent and permanent guidance during the elaboration and realization of this doctoral thesis. I also thank him for his support in writing scientific articles published in specialized journals.

Thanks to the chair of the doctoral committee, Prof.univ.habil.dr.ing. Florin Miculescu and distinguished official referees, members of the doctoral committee: Prof.univ.dr.ing. Petrică Vizureanu, from the Technical University of Iaşi, prof.univ.dr.ing. Mircea Nicoara, from the Polytechnic University of Timişoara and Prof.univ.dr.ing. Brandusa Ghiban, from the Polytechnic University of Bucharest, for the honor of reviewing this paper.

This doctoral thesis would not have been complete without the essential support and help of some teachers from the Faculty of Materials Science and Engineering, Polytechnic University of Bucharest, respectively Prof.univ.habil.dr.ing. Florin Miculescu, Conf.dr.ing. Cosmin Cotruț, Conf.dr.ing. Andrei Berbecaru, S.L.dr.ing. Robert Ciocoiu, S.L.dr.ing. Octavian Trante. I thank them for their time, help and valuable scientific advice.

Cordial thanks to Prof.univ.dr.ing. Corneliu Munteanu and Conf.dr.ing. Bogdan Istrate from „Gheorghe Asachi" Technical University of Iasi for their support in the realization of this thesis on aspects of improving corrosion resistance of experimental samples by coating with alumina using the deposition by plasma spraying performed in the present doctoral thesis.

Thanks to all fellow PhD students, teachers from the Department of Metallic Materials Science Physical Metallurgy, Faculty of Materials Science and Engineering, Polytechnic University of Bucharest, all friends who encouraged and supported me. With great gratitude and love, I dedicate this thesis to my family, who stood by me and supported me in every way during this period.

CONTENT

INTRODUCTION

In this doctoral thesis, attention has been focused on the field of metallic materials used in road vehicle body elements, in particular on metal body elements that have been involved in road accidents and that have resulted with deformations of these parts and have been subsequently reconditioned and put into function again. Due to the existing situation at the level of road accident assessment, it was found that in the case of technical examinations following road accidents the difference between metal body elements reconditioned after previous plastic deformations and metal body elements that did not suffer plastic deformations is not taken into account. Starting from this premise, it is tried to show that the mathematical models used in the assessment of road accidents should also include the material aspects related to metal body elements, respectively microstructural aspects, the history of thermo-mechanical processes suffered by these elements during operation and mechanical properties.

The objective of this paper was to evaluate the efficiency of reconditioning by various thermo-mechanical processing technologies and plasma jet coatings of metal body elements involved in road accidents that led to deformations of these parts, through microstructural investigations, determination of mechanical characteristics and corrosion resistance.

The structural and mechanical evaluation of some experimental parts taken from metal body elements from crashed vehicles (same type of body element and same car manufacturer) was performed in order to compare different reconditioning methods, respectively:

- reconditioning methods by cold plastic deformation;
- reconditioning methods by hot plastic deformation, heating with oxyacetylene flame;
- reconditioning methods hot plastic deformation, induction heating;
- reconditioning methods by hot plastic deformation, heating using the "spotter" technique.

Through these plastic deformation processes which consist in straightening the car panels by different methods, the influence of the material factor at the moment of a road accident is highlighted. Subsequently, an innovative method was tried in the field of reconditioning metal body elements from crashed vehicles, respectively coating them with alumina (Al_2O_3) by plasma spraying.

This doctoral thesis is structured in two main parts, namely the theoretical part and the experimental part. The first part represents the theoretical support and the fundamental basis of this work and includes two main chapters.

Chapter 1, entitled „Current status in the field of metallic materials used in the automotive industry" presents in detail the type of materials used for certain parts of a car and also the properties that recommend these materials for use in the automotive field. Also, two important aspects to follow in this paper are the processing of metal body elements subjected to road accidents and their processing methods, aspects that are addressed in this chapter.

Chapter 2 „Road accidents. Factors influencing road accidents and their assessment methods" focuses on road accidents, the factors that influence road accidents and methods of assessing road accidents. This chapter is essential in order to investigate the factors that cause a road accident and to analyze the importance of the material factor at the time of accidents.

Next, the experimental part will be briefly presented, which consists of a number of 4 chapters.

So, in **chapter 3** named „Materials, analysis techniques, test methods and equipment used experimentally" the objective of this doctoral thesis, the work plan, the materials used, as well as the methods and techniques of analysis used to obtain the experimental results are presented in

detail. For this study, metal body elements were obtained from cars of the same type and the same manufacturer involved in similar collisions that showed a similar degree of deformation. These samples were straightened using specific workshop procedures for cold and hot straightening using the hammer and by heating using the flame and inductor.

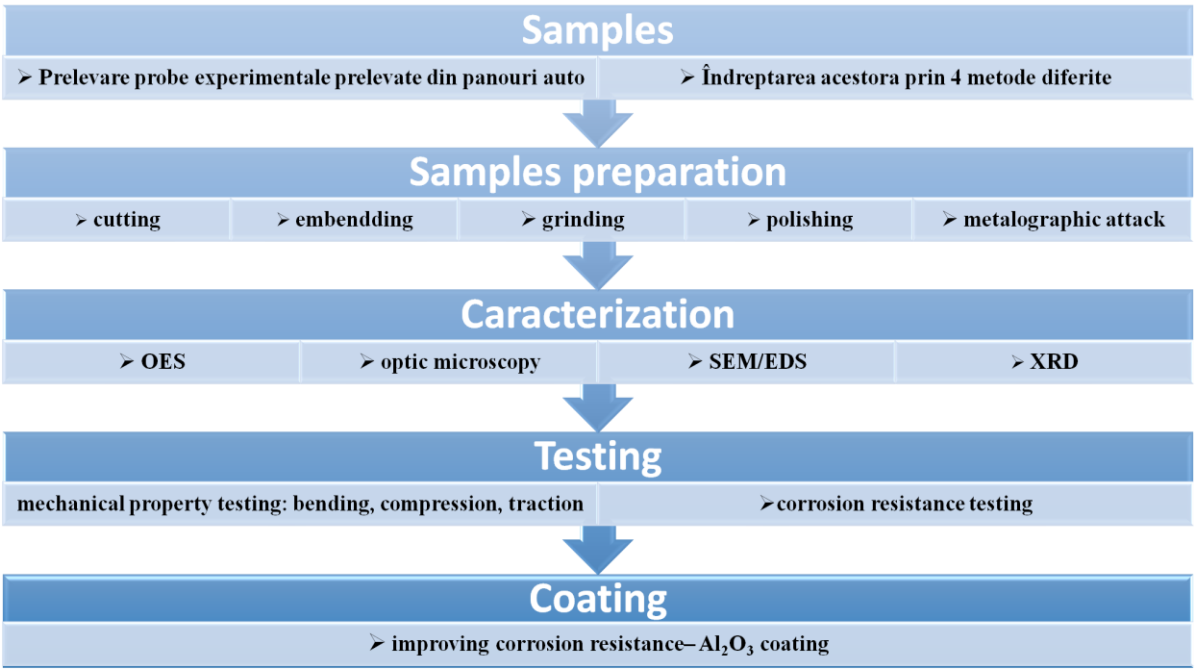

Fig. 3.1: Scheme of the work plan for the experimental samples obtained

Chapter 4 named „Preliminary study to investigate the influence of plastic deformation methods on the mechanical properties of some car body elements" represents the initial studies on which this doctoral thesis is based and consists in determining the mechanical properties of some self-treated and plastically deformed car body elements.

Chapter 5 named „Microstructural characterization, determination of mechanical properties and corrosion resistance" aims to highlight the microstructural aspects by optical microscopy, scanning electron microscopy, EDS spectrometry, and X-ray diffraction. This chapter also includes the mechanical characterization of the analyzed materials by determining the microhardness, tensile strength and compressive strength. At the same time, the surface properties are determined by measuring the contact angle and the physico-chemical properties by determining the corrosion resistance using the electrochemical method.

In **chapter 6** „Improving the corrosion resistance of experimental samples by coating with alumina using plasma spraying deposition" the experimental samples coated with Al_2O_3 are coated in order to improve the corrosion resistance and the results obtained after their characterization are presented by the same techniques and methods as in the previous chapter, to highlight the differences between coated and uncoated materials.

This doctoral thesis ends by presenting the conclusions reached in this doctoral thesis, as well as personal contributions to it.

The continuation of this summary presents the experimental results obtained.

CHAPTER 4: PRELIMINARY STUDY TO INVESTIGATE THE INFLUENCE OF PLASTIC DEFORMATION METHODS ON THE MECHANICAL PROPERTIES OF SOME CAR BODY ELEMENTS

The main purpose of this chapter is to investigate the influence of different methods of plastic deformation on the mechanical properties of materials. For this purpose, experimental samples were collected from two regions of the car body, namely: from the proximity of the car door ('Door') and from the central region of the panel ('Side panel').

4.1. Determination of tensile strength

The following figure shows, comparatively, the voltage-deformation curves obtained from the traction test for each sample obtained and processed.

According to the diagrams in figure 4.1, the appearance of stress-strain curves indicates ductile behavior with significant plastic deformations. A particular aspect is the appearance of the yield strength in the case of test samples obtained from hot plastic deformed panels. In the case of test samples obtained from the original panel, the absence of this detail suggests that the steel is deformed plastic, and by heating it is observed the similar effect to a annealing heat treatment, which leads to the recurrence of the apparent yield strength. Similar behaviour can be observed for experimental samples obtained from the proximity of the door. Thus, the behavior of steel is ductile, with significant plastic deformations, and in the case of heated samples the occurrence of the flow point phenomenon is observed.

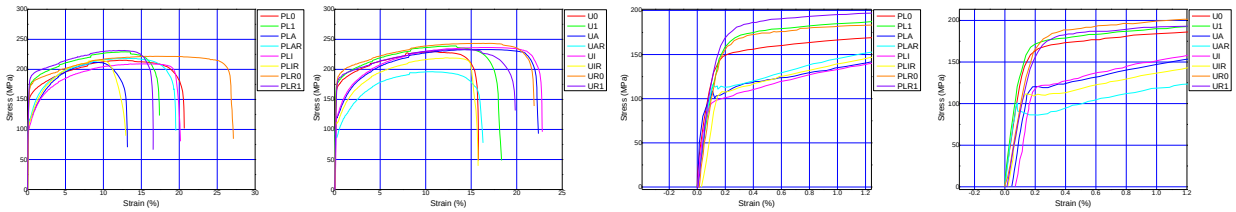

(a) (b)

Fig. 4.1: Characteristic curves of the test samples obtained from the side panel and the proximity of the door indicating: (a) the overall aspect and (b) the detail of the flow region

Comparisons of the mechanical properties made between the samples obtained from the side panel and those obtained from the proximity of the door are shown in the following figure.

PL0 and PL1 have close values of the lateral contractions. PLA, PLI and PLR0 show a decrease in the lateral contractions. PLR1 shows an increase in this parameter, which suggests an induced structural non-homogeneity. The U0 and U1 samples have close values, and the UA doesn't show a variation in the value of the lateral contractions, in contrast for UAR and UI there is a decrease in this parameter. The UIR doesn't show a significant change in the lateral contractions, but a structural non-homogeneity is noted.

The values of the percentage elongation at fracture are close in the case of the initial samples. Warming leads to an increase in elongation, but for the PLA sample there is a decrease in elongation. In the case of cold plastic deformation, the samples obtained from the side panel show an irregular variation, while in the case of samples taken from the proximity of the door, an increase in elongation occurs.

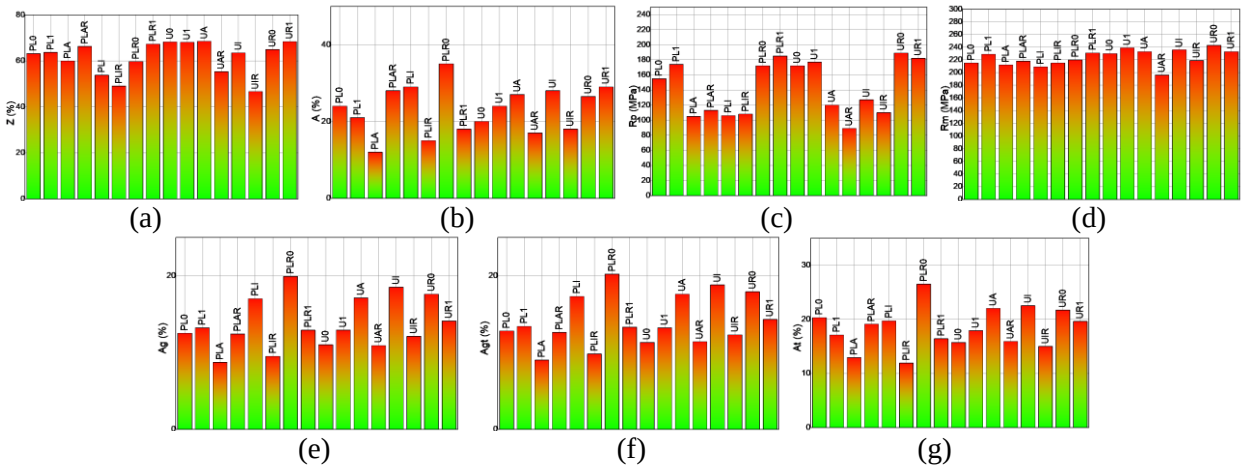

Fig. 4.2: Variation of the mechanical properties of the experimental samples tested for traction: (a) variation of the lateral contractions; (b variation of the percentage elongation at fracture; (c) the area of the yield strength; (d) variation of the mechanical strength; (e) variation of the non-proportional elongation under the maximum force; (f) variation of the total percentage elongation under the maximum force; (g) variation of the total percentage elongations at fracture

The yield strength for PL0 and PL1, U0 and U1 samples have approximately equal values between them. Cold plastic deformation increases the yield strength by ecrusing the material. The heating of the material produces a decrease in the yield strength.

The variation in mechanical resistance is not a significant one, it varies between 196 MPa for the UAR samples and 243 MPa for the UR0. With the exception of the UAR, experimental samples obtained from the proximity of the door show higher values of mechanical tensile strength compared to the samples in the side panel.

As regards non-proportional elongation under the maximum force, there is a tendency to increase in cold plastic deformated samples and an irregular variation in heated samples, in the sense that the values either increase or decrease. The change in the total percentage elongation under the maximum force is similar, with values being approximately 3-4% higher than in the previous case. With regard to the total percentage elongation, a decrease is observed in the case of reconditioned samples by hot plastic deformation.

4.2. Study of local deformations in samples

Comparing the lengths of the PL0 and PL1 samples, high length values in the breaking area are noted with a gradual transition to the extremities, indicating a uniform pick-up of the stresses. Lateral contractions have higher values in the fracture zone and a gradual transition to the extremities.

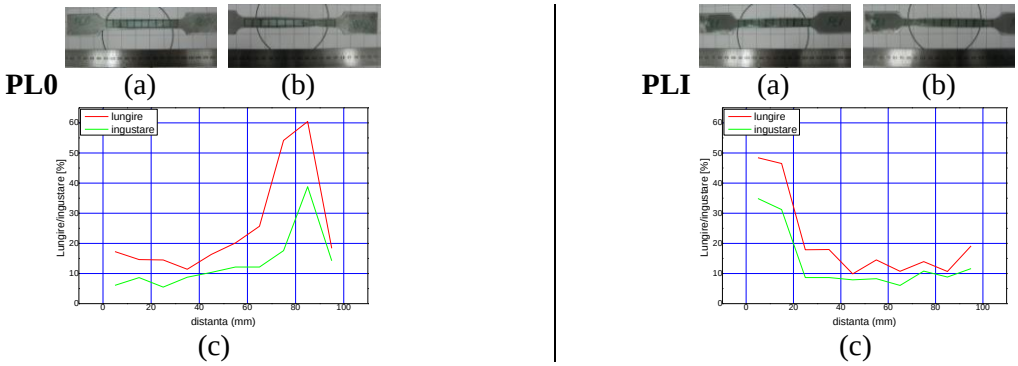

Fig. 4.3: Fig. 4.3: PL0 and PL1 samples with grid surface – (a) before the traction test; (b) after the traction test; and (c) variation in length and lateral contractions by distance

In the case of the PLA sample, there is a sudden increase in lengthening and lateral contractions in the fracture area, the rest of the sample being less mechanically stressed. In the case of the PLAR sample, there is a gradual decrease in lengthening and lateral contractions, which suggests a uniform distribution of mechanical stresses.

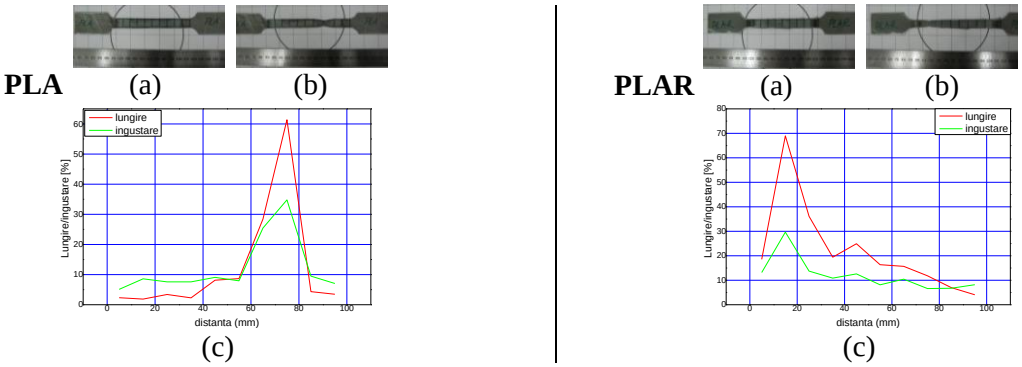

Fig. 4.4: PLA and PLAR samples with grid surface – (a) before the traction test; (b) after the traction test; and (c) variation in length and lateral contractions by distance

The lengths of the PLI samples gradually decrease throughout these, but the lateral contractions are larger. In the case of the PLIR sample, two distinct regions in which stresses are concentrated, have a relatively uniform distribution. The lateral contractions gradually increase to the fracture zone.

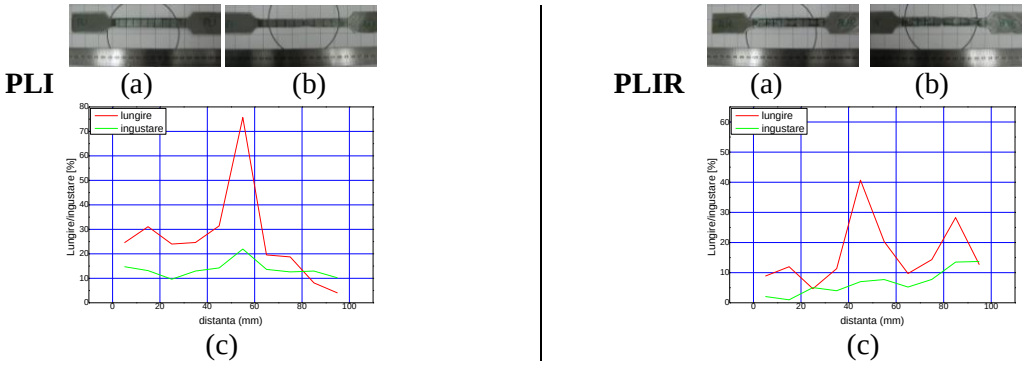

Fig. 4.5: PLI and PLIR samples with grid surface – (a) before the traction test; (b) after the traction test; and (c) variation in length and lateral contractions by distance

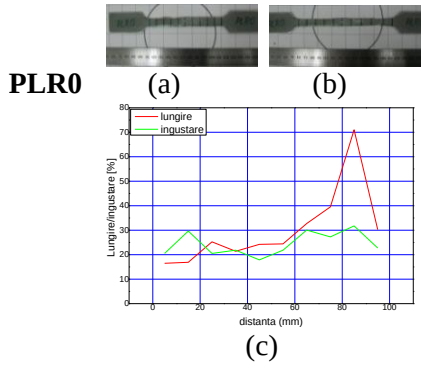

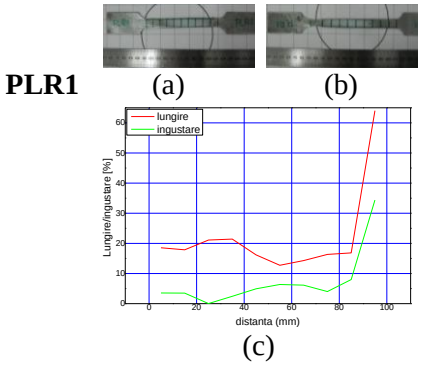

Fig. 4.6: PLR0 and PLR1 samples with grid surface – (a) before the traction test; (b) after the traction test; and (c) variation in length and lateral contractions by distance

The variation in the lengths of the U0 and U1 samples is similar and a gradual decrease is observed from the fracture area to the extremities. Lateral contractions indicates a gradual transition from the fracturearea to the extremities, indicating a uniform takeover of mechanical stresses.

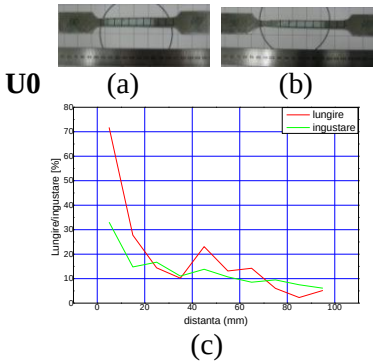

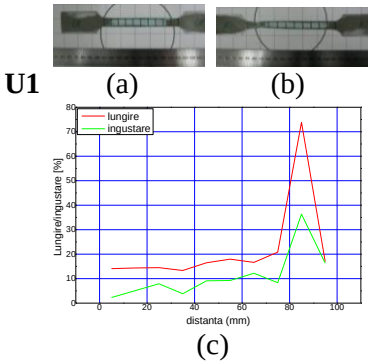

Fig. 4.7: U0 and U1 samples with grid surface – (a) before the traction test; (b) after the traction test; and (c) variation in length and lateral contractions by distance

The UA samples has concentrated lengthening in two regions and causes stronger deformities. The stresses isn't uniform distributed in the material. Strong deformities occur in the fracture region of the UAR sample, with a gradual decrease towards the extremities, indicating a more uniform demand.

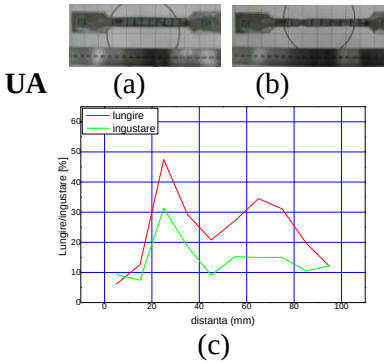

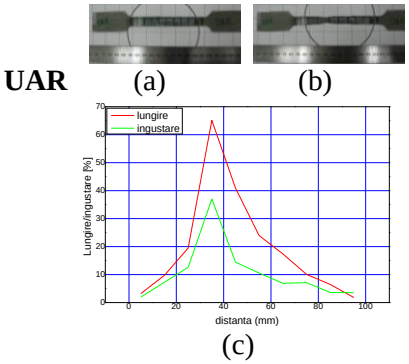

Fig. 4.8: UA and UAR samples with grid surface – (a) before the traction test; (b) after the traction test; and (c) variation in length and lateral contractions by distance

The UI samples has a distribution of lengthening and lateral contractions similar to the UA, but the values in the fracture zone are significantly higher with a single concentration of stresses. The UIR samples shows a uniform overtake of stresses, with considerably lower lateral contractions.

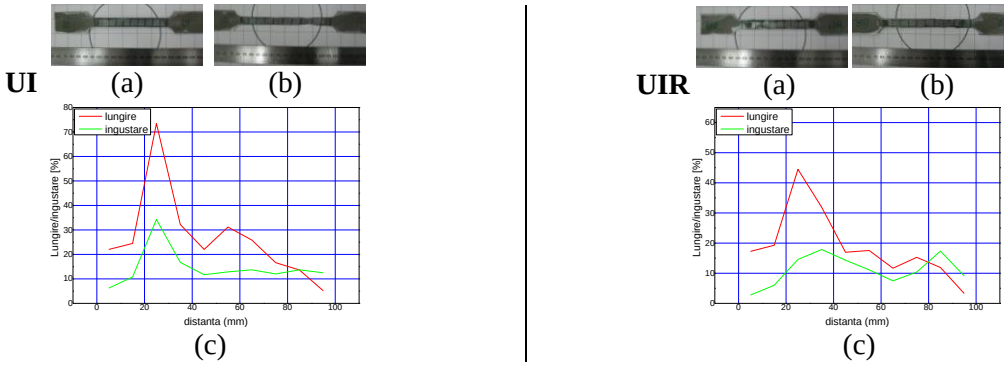

Fig. 4.9: UI and UIR samples with grid surface – (a) before the traction test; (b) after the traction test; and (c) variation in length and lateral contractions by distance

UR0 and UR1 samples show strong deformities in the fracture area with a sudden transition. The variation in lateral contractions is similar to U0 and U1 samples, but areas with a higher concentration of stresses occur.

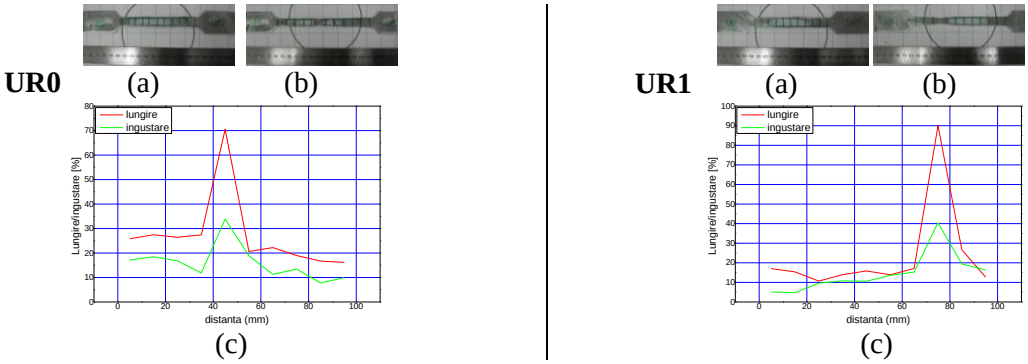

Fig. 4.10: UR0 and UR1 samples with grid surface – (a) before the traction test; (b) after the traction test; and (c) variation in length and lateral contractions by distance

CHAPTER 5: MICROSTRUCTURAL CHARACTERIZATION, DETERMINATION OF MECHANICAL PROPERTIES AND CORROSION RESISTANCE

The microstructural characterization of the experimental samples was aimed at highlighting the microstructural aspects through optical microscopy, scanning electron microscopy, EDS spectrometry, and X-ray diffraction. The morphology of the internal microstructure of the material, the size of the grain, the analysis of the content of inclusions, the phases and compounds of the internal structure of the material were followed.

5.1. Optical microscopy determinations

5.1.1. Analysis of the content of inclusions

The study of inclusions was carried out on experimental samples analysed in the longitudinal section. Non-metallic inclusions were found to exhibit an non-homogeneous distribution in the base metal mass with considerable dimensional variation. Looking at the layout of the inclusions, they present a preferential orientation towards the direction of plastic deformation.

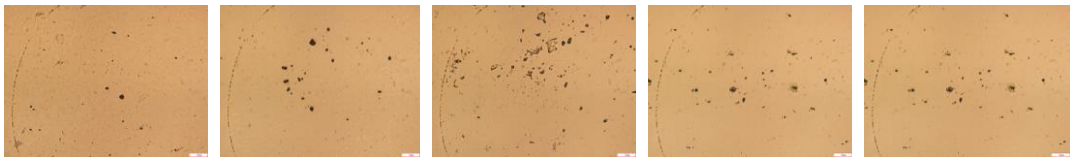

P1 P2 P3 P4 P5

Fig. 5.1: Inclusio's content studied on longitudinal direction of the samples

5.1.2. Microstructure analysis

The microstructure was highlighted using the nital metalographic reagent with a concentration of 2%. The studies were carried out in both a longitudinal and transversal direction. The majority structural constituent that can be identified in the micrographs presented is ferrite with the presence of a compound defined on the grain limit - tertiary cementite. Visual inspection and grain size do not show clear dimensional variations, which validates the efficiency of the procedure implemented, following controlled heating there is no significant dimensional variation.

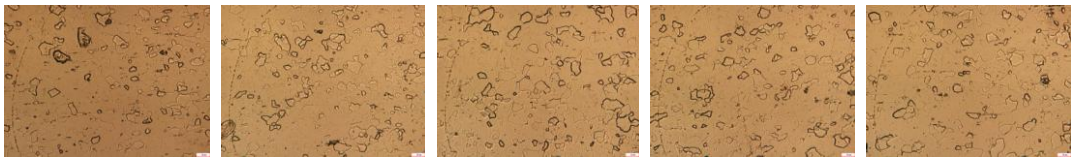

P1 P2 P3 P4 P5

Fig. 5.2: Micrografiile eșantioanelor experimentale pe direcție longitudinală, atac: nital 2%

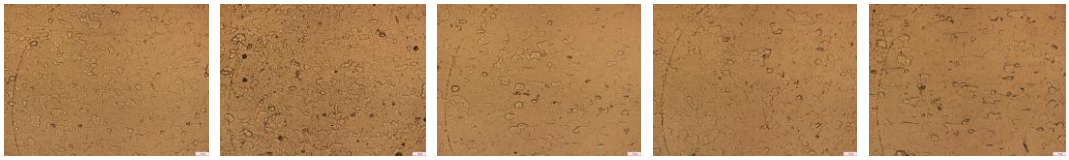

P1 P2 P3 P4 P5

Fig. 5.3: Micrografiile eșantioanelor experimentale pe direcție transversală, atac: nital 2%

5.1.3. Determination of grain size

Figure 5.4 shows an extract from the analysis bulletin generated for the analysis of the steel samples taken from the original automotive panel (sample P1), in which it can be observed that the average grain size is 10.39.

.

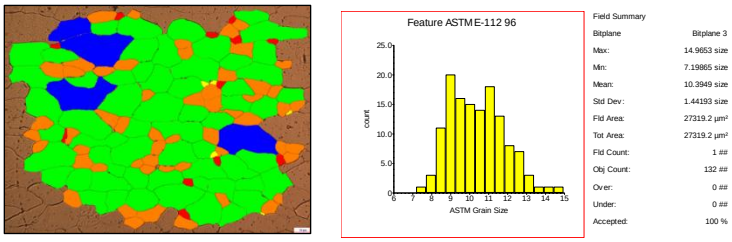

Fig. 5.4: Extras din buletinul de analiză generat pentru proba P1

In the case of the steel sample obtained from the recondionated panel by heating with oxyacetylene flame (sample P3) the analysis was carried out on the region with the highest granulation. The grain size is 6.34.

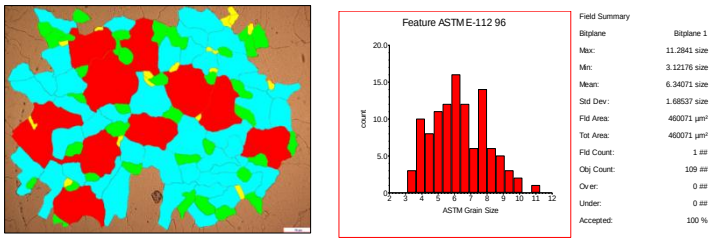

Fig. 5.5: Extras din buletinul de analiză generat pentru proba P3

Similar to the study of the previous sample, the grain size of the steel sample obtained from the heated panel using an inductor (sample P4) was determined in the region with the highest granulation, the result being presented in the extract in the analysis bulletin in figure 5.5.

The application of the Heyn method involved establishing a region of interest, placing a grid of horizontal lines and identifying their points of intersection with the grain boundary. In fig. 5.6, the results of the analysis for sample P3 and sample P4 are presented in comparison.

(a) 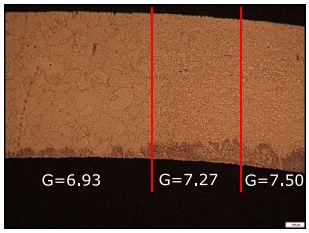

(b) 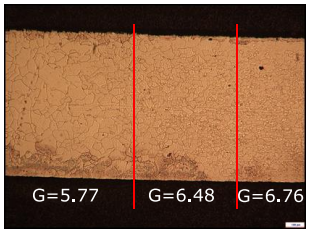

Fig. 5.6:Mărimea de grăunte în diferite regiuni pentru: a) proba P3 și b) proba P4

Given that the initial grain size was G=10.39, there is a sharp increase in the region where the heat flow was maximum and a gradual increase with the increase in distance from this region.

It can be said that in the case of samples obtained from metal parts involved in road accidents which have been reconditioned by hot plastic deformation, induction heating (sample P4), the increase in austenitic grain is more pronounced, most likely due to the faster heating speed.

In the light of this study, the acccentuation of anistropy and structural non-homogeneity of the material was found, which leads to mechanical behavior difficult to estimate due to uneven states of tension and deformation in the material.

5.2. Determination of scanning electron microscopy (SEM) and energy dispersive X-ray spectroscopy (EDS)

The following figure shows the SEM missorographs for the P1 sample at different magnifications to highlight the grain and their distribution. It can be observed that the images are characterized by grain with different dimensions. The micrograph shown in Figure 5.7 (c) was processed using the ImageJ program to characterize grain size. The results of this analysis (Fig. 5.7 (d) and (e)) show that the average grain size is 7.36 μm, characterized by an average grain area of 58.04 μm^2.

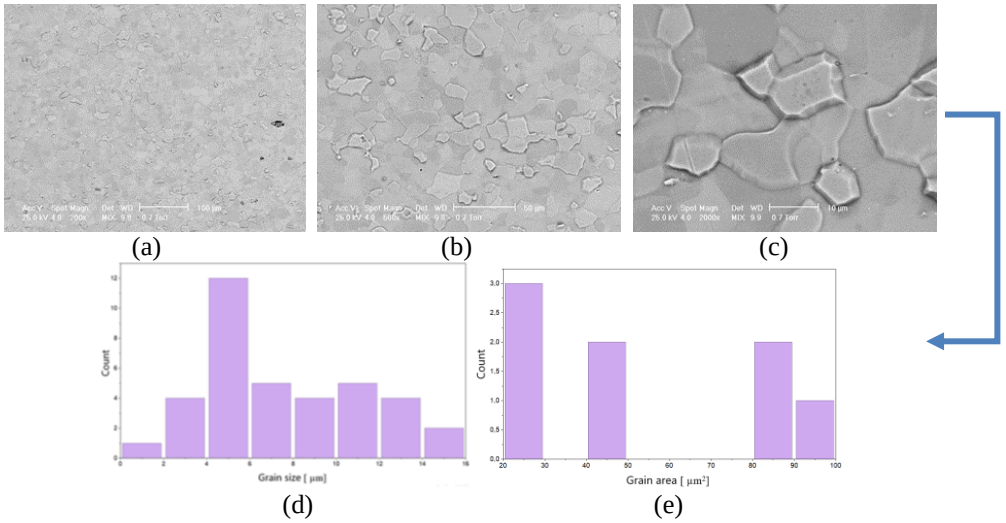

Fig. 5.7: SEM micrographs for sample P1, attack: nital 2%, at magnification of: (a) 200X; (b) 500X; (c) 2000X and analysis of the micrography grain size (c) using the Image J programme with which the grain sizes (c) and grain areas (d)

Figure 5.8 shows the SEM imgages for the P2 sample, in which a variety can also be observed in terms of grain sizes. The results of the analysis of the grain size analysis obtained from the analysis of the micrograph shown in Figure 5.8 (c) confirm this, as the grain size is in the range of 1.71 μm and 12.69 μm, with the average grain size of 7.67 μm.

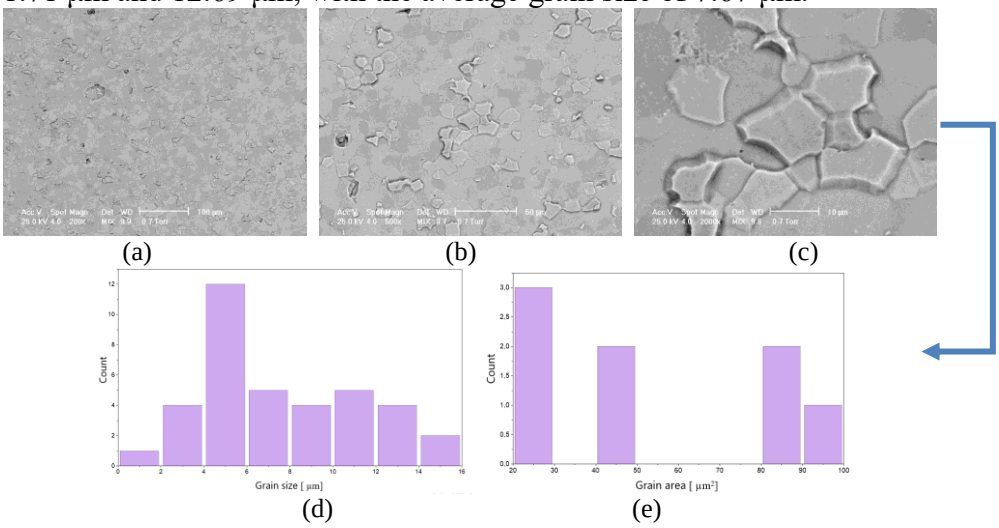

Fig. 5.8: SEM micrographs for sample P2, attack: nital 2%, at magnification of: (a) 200X; (b) 500X; (c) 2000X and analysis of the micrography grain size (c) using the Image J programme with which the grain sizes (c) and grain areas (d)

The following figure shows the results of the SEM and those obtained from the analysis of the grain size for sample P3. It can also be observed that in this case there is a non-uniformity of grain size, ranging from 3.07 μm to 58.4 μm.

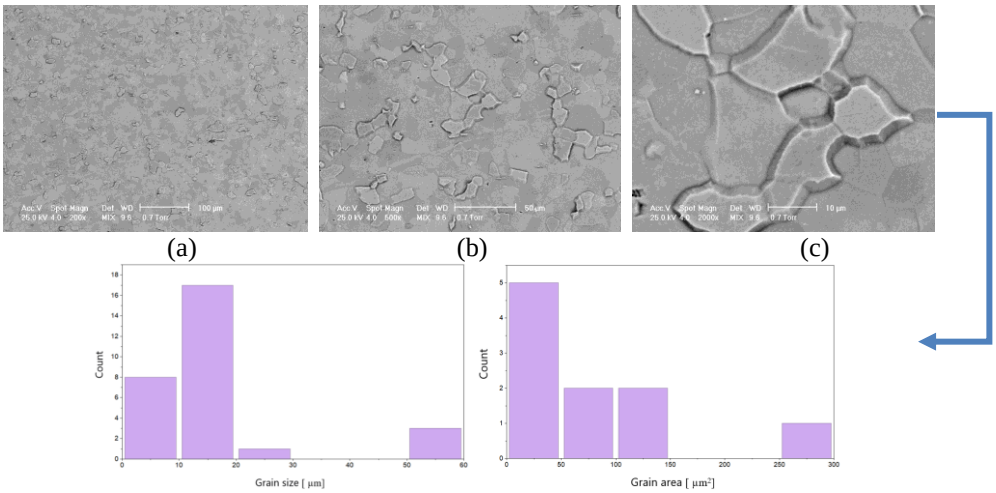

Fig. 5.9: SEM micrographs for sample P3, attack: nital 2%, at magnification of: (a) 200X; (b) 500X; (c) 2000X and analysis of the micrography grain size (c) using the Image J programme with which the grain sizes (c) and grain areas (d)

In the case of the induction heating sample (sample P4), shown in the following figure, a pronounced increase in grain size can be observed than in the previous case up to an average value of 9,92 μm.

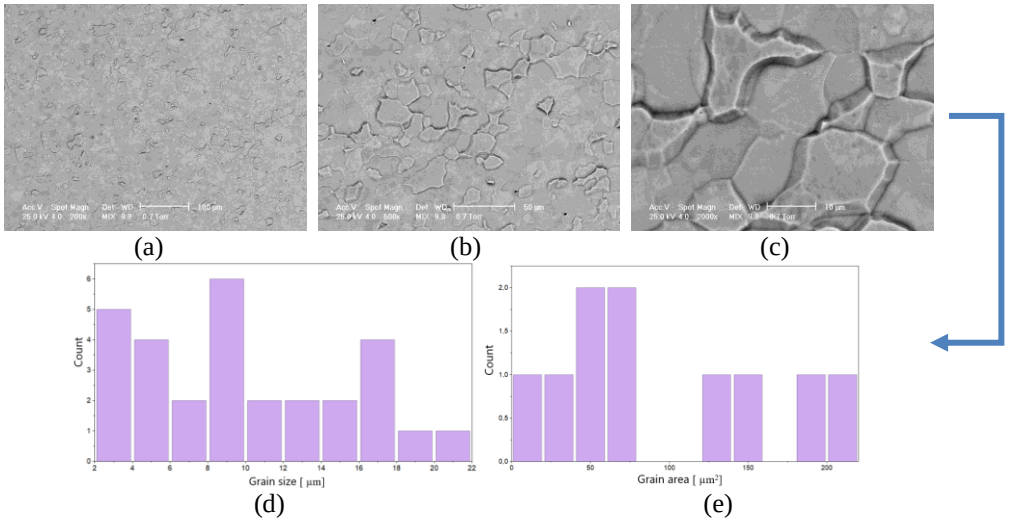

Fig. 5.10: SEM micrographs for sample P4, attack: nital 2%, at magnification of: (a) 200X; (b) 500X; (c) 2000X and analysis of the micrography grain size (c) using the Image J programme with which the grain sizes (c) and grain areas (d)

The P5 sample (reconditionated by the "spotter" method), shown in Figure 5.11, has a behaviour similar to the P3 sample (reconditionated by induction heating), since the mean values of the grain size obtained from the analysis are approximately equal, but in this case the grain size is of greater uniformity, ranging from 2.09 to 16.05 μm.

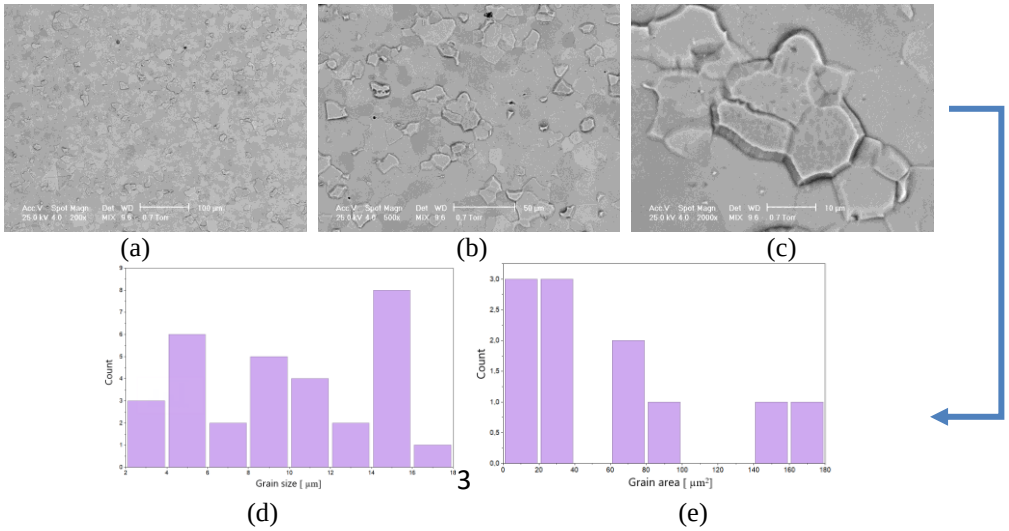

Fig. 5.11: SEM micrographs for sample P5, attack: nital 2%, at magnification of: (a) 200X; (b) 500X; (c) 2000X and analysis of the micrography grain size (c) using the Image J programme with which the grain sizes (c) and grain areas (d)

This study confirmed a slight increase in grain size for samples directed by: ociaacetylene flame heating (sample P3) and induction heating (sample P4), but the increase is not a significant one so as to drastically affect the mechanical characteristics of the alloy. Studies and research by optical and electronic microscopy have validated the effectiveness of the heating procedure proposed and implemented in this study.

Since all the experimental samples were obtained from similar automotive panels of the same chemical composition and the mechanical processing methods did not have an effect on the chemical composition of the materials, the EDS (Energy-Dispersive X-Ray Spectroscopy) analysis was carried out on a single sample.

The figure below shows a representative SEM image (at a magnification of 3000X) of the P3 sample and the map of the chemical elements found on the surface of the sample to highlight their distribution, as well as the EDS graph.

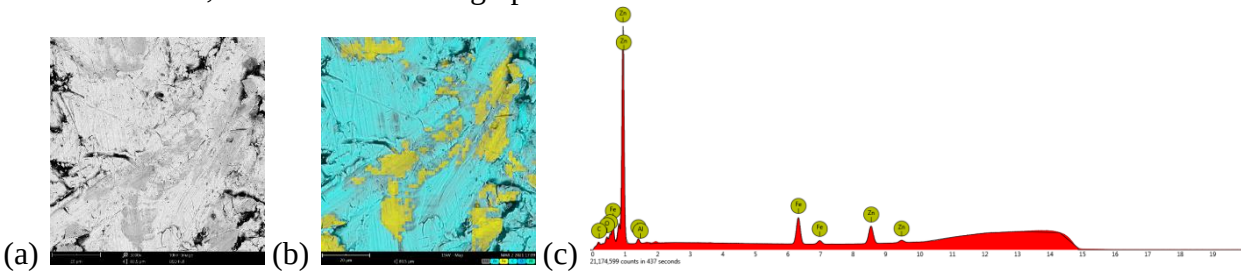

Fig. 5.12: The results of the SEM and EDS analysis for the representative sample P3: (a) SEM micrography of the area on which the EDS analysis was carried out; (b) the map of the constituents and their distribution; (c)the graph of the distribution of the elements

5.3. X - ray diffraction determinations

X-ray diffraction analyses were carried out to determine the existing constituent phases of the samples analysed. This analysis is presented by overlapping difractograms in 2D plane (Fig. 5.13).

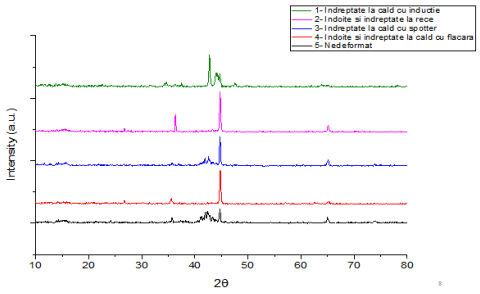

Fig. 5.13: Comparative analysis of difractograms by the overlaying

The indexing of X-ray difractograms using the ICCD PDF 4 database can be used to ensure that in the case of P1, P4 and P5 samples the constituent phases are ferrite (α) and austenite (γ), and the P2 and P4 samples have a single constituent phase, namely ferrite (α).

Due to the fact that the basic material has been used to mechanical deformation processes by several techniques, it can be observed that for reconditionated materails by spotter and by heating with induction, in the structure of samples, in addition to the ferrite also appears austenite. In the case of reconditionated samples by cold deformatioan and by heating with oxyaacetilene flame, no structural changes in the mass of the material shall be detected.

5.4. Determination of mechanical properties

5.4.1. Determination of Vickers microhardness

Microdurity determinations were performed in accordance with *ISO 6507-1 Metallic materials - Vickers Hardness Test - Part 1: Method test* on all 5 types of experimental samples (P1, P2, P3, P4, P5) using a microdurimeter produced by CV Instruments. A load of 200 g and a maintenance duration of 30 s was used. The results are centralized in the form of a bar graph shown in Figure 5. 14.

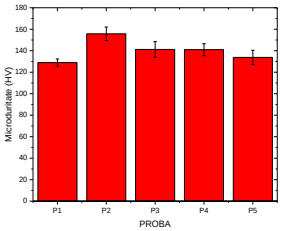

Fig. 5. 14: Average microdurity value for each experimental sample

Analyzing the average values of microdurity it is found that there are no statistically significant differences between the P1 (sample obtained from the original panel) and P5 (sample obtined from the spotter-reconditionated panel) and there are no statistically significant differences, the values being close. The highest value of microdurity occurs in the case of the P2 (sample obtained from metallic car body elemets involved in road accidents that have been deformed and reconditionated by cold plastic deformation)

More particular behaviour is consistent with P3 and P4 samples which, although heated, show an increase in hardness compared to the initial state (sample P1). This behavior can be explained by the fact that the adoption of a strictly localized heating causes the material to expand locally, and the presence of strong stresses produced in the material due to dilation and contraction (especially during cooling) leads to a plastic deformation located in the heated region and immediately adjacent to it.

The previous study, in which the heated surface was considerably larger and the temperature and duration of maintenance unchecked, led to a uniformity of temperature in the material, which is why cooling occurs uniformly, resulting in a uniformity of the microstructure which manifests itself in unit values of hardness.

5.4.2. Determination of tensile strength

The appearance of the curves corresponding to the P1 sample indicates ductile behaviour with significant plastic deformation. The lack of apparent yield strength suggests that the material is in a structural state other than that ofequilibrium.

The appearance of cold plastic deformed saples (sample P2) induces ductile behaviour with significant plastic deformation. The behavior depends on the orientation of the test tube towards the direction of deformation of the material, thus confirming the anisotropy of the material.

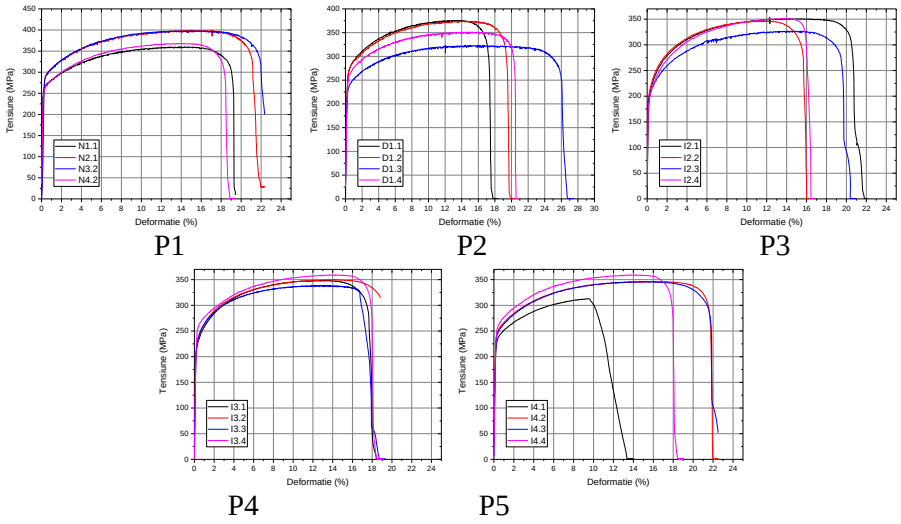

Fig. 5.15: Fig. 5. 15: Characteristic curves for experimental samples

Ccharacteristic urbs obtained from the traction test of hot-deformed experimental plastic samples using as a heat source the oxyacetylene flame (sample P3), suggests a ductile material with significant plastic deformation preceding the rupture. Compared to previous cases anisotropy is less pronounced.

The appearance of the curves of the P4 sample (hot plastic deformation by induction) suggests a ductile material, the plastic deformations are considerable until breaking. Anisotropy is removed if reference is made to samples in previous structural states.

The appearance of the curves characteristic for the samples deformed by the "spotter" method indicates a behaviour similar to the P4sample. And in this situation the effect of anisotropy is significantly reduced.

Variation in mechanical strength shown in Figure 5. 16 (a) shows a continuous decrease in values, the highest value being observed in the case of reference sample P1. In the preliminary study it was stated that this parameter is not the most suggestive descriptor of mechanical behavior due to structural unevenness and states of tension and deformation. Mechanical strength values range from 341 to 382 MPa, with a range of 41 MPa. The most suggestive parameter for the mechanical characteristics of the sampls was considered the yield strength of the material, its variation being indicated by fig. 5.16(b), which has the highest value in the case of theP1 re-safe sample, followed by samples P2 and P5. The samples directed by heating show significantly lower values.

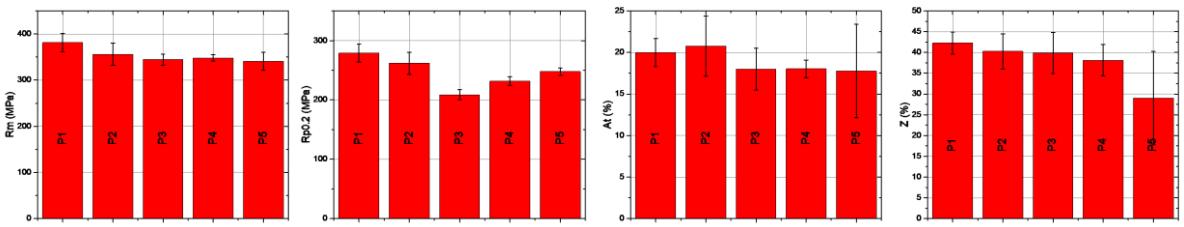

(a) (b) (c) (d)

Fig. 5.16: Comparisons between the average mechanical characteristics of the samples, a. mechanical strength, b. yield strength, c. breaking elongation and d.

For a better view of the distribution of voltages and deformations in a test tube subjected to an axial traction stresses, an assembly composed of 4 zones has been created that shapes the grain-sized gradient areas observed by optical microscopy.

Figure 5. The design shall be presented in which, for simplification, a central area (component 1), of circular shape, representing the area in direct contact with the heat source and which has presented a grain with a maximum average diameter and, consequently, the mechanical characteristics have been set up in the programme as the smallest.

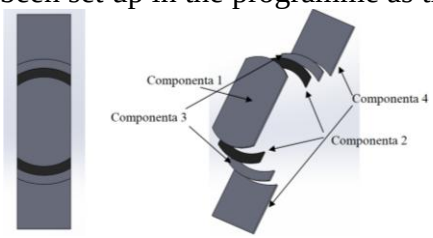

Fig. 5.17: Overview of the constructive details of the model

Component 2 and component 3 are areas where the grain size is intermediate to Component 1 and the base alloy (component 4), considering the average grain diameter for component 2 larger than for component 3 and thus the mechanical characteristics being set up accordingly. Synthetically, in terms of the value of the yield stregth, we can describe the setting up of the mechanical characteristics of the model by inequality:

$$Rp_{0,2component\ 4} > Rp_{0,2component\ 3} > Rp_{0,2component\ 2} > Rp_{0,2component\ 1} \quad (5.1)$$

Once the geometries and material characteristics of the components were defined they were combined in the form of a solid (obviously, excessive simplification of the model led to the removal of some grain-sized gradients, but in order to reduce the preprocessing and processing

time of the simulation these omissions were considered necessary) on which a constraint and an axial traction demand was applied.

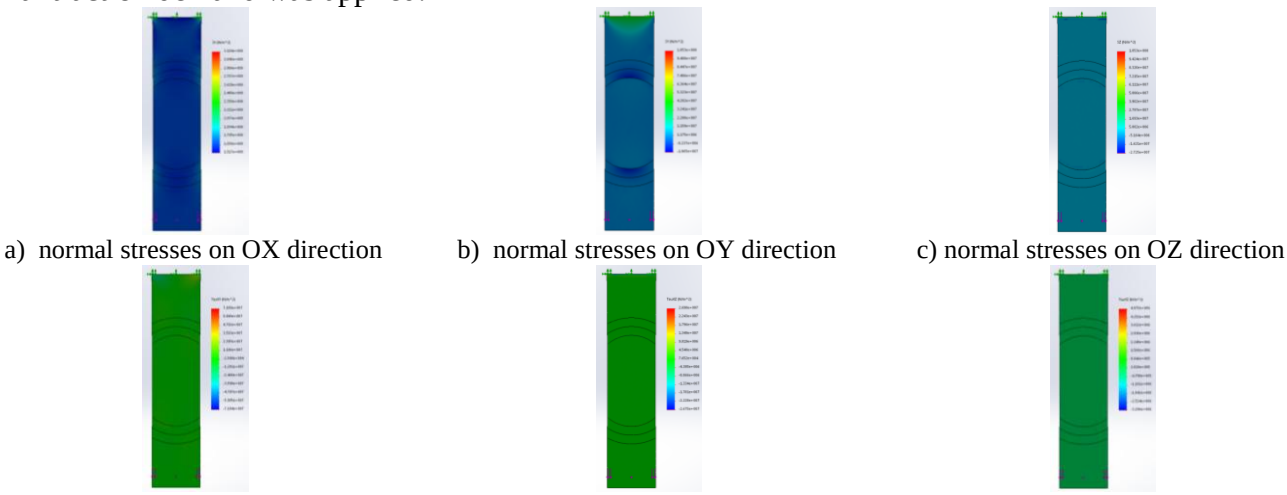

a) normal stresses on OX direction b) normal stresses on OY direction c) normal stresses on OZ direction

d) shear stresses on XYdirection e) shear stresses on XZ direction f) shear stresses on YZ direction

Fig. 5.18: Distribution of mechanical stresses according to the analysis carried out

The post-processing phase was mainly aimed at the distribution of tensions and deformations in the whole. Thus the figure above shows the distribution of tensions as a whole and a relatively uniform distribution of them is observed, with slight variations depending on the direction in which the analysis was carried out.

As regards the distribution of deformations in the whole, in Figure 5. 19 is found to be uneven, Figure 5. 19 (c) and 5. 19. d) highlighting this by making deformation isosections.

Deformation energy, Figure 5. 20 (a) and its density, Figure 5. 20 (b), confirms the uneven distribution of deformations as a whole.

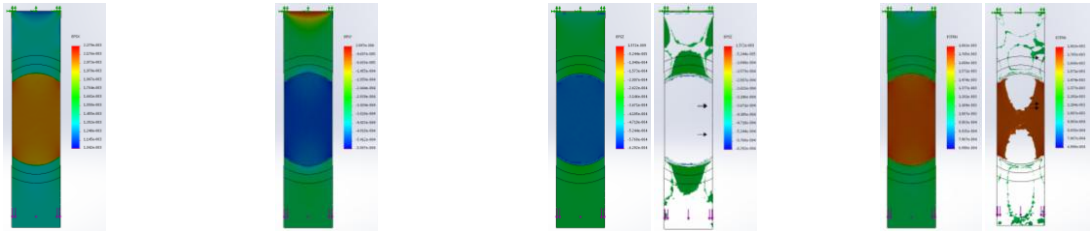

(a) deformation on OX; (b) deformation on OY; (c) deformationon OZ; (d) equivalent deformations

Fig. 5.19: Distribuția deformațiilor din ansamblu conform analizei

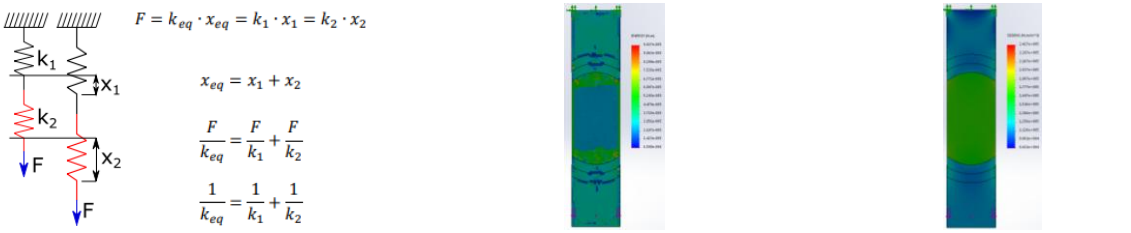

(a) the behavior of series springs (b) deformation's energy (c) deformation's energy density

Fig. 5.20: Distribution of deformation energy and its density

Basically, by exceeding the value of the elasticity limit, considerably lower in regions with a large grain diameter, these areas will enter the plastic region more quickly, overforming the other areas of the assembly, and the uneven deformation is installed much faster.

By modifying the states of tension and deformation in these regions, the ideal premises are created to prime the fissure and rupture, aspects also noted in the experimental determinations of mechanical behavior.

The description of the mechanical behaviour of the experimental samples, due to the unevenness of the stresses and deformation, must call on both the appearance of the stress-strain curves and the characteristics determined on the basis of them, in this case the elongations at breakage, the damage and the yield strength.

In the case of reference sample, the existence of a pronounced anisotropy is found, the mechanical characteristics being strongly conditioned by the direction of application applied to the material. Voltages and deformations shall be evenly distributed throughout the length as shown in Figure 5.21 (a), uneven states occur only in the heavily damaged region, where tearing occurs (Fig. 5.21 (b)).

Cold plastic deformation shows a decrease in anisotropy associated with an artificial increase in breaking elongation and decrease in yield strength. This behavior can be explained by inducing a state of uneven tension and deformation: zonal material is strongly ecruised, these regions become voltage concentrators (Fig. 5. 22 (a)), the test tube is no longer evenly strained, the yield stragth begins to decrease, and due to the impossibility of perfect straightening, spontaneous "straightening" occurs during the axial demand, artificially increasing the yield stregth. These claims are supported by a decrease in necking in the breaking area.

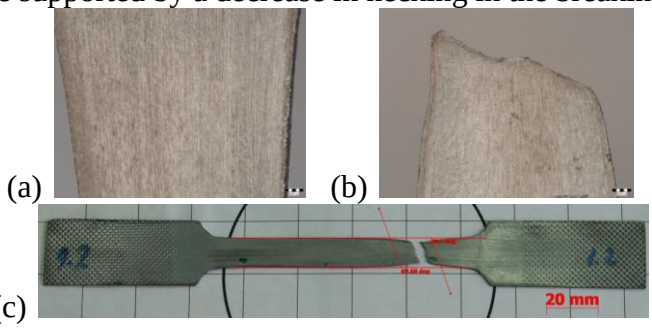

Fig. 5.21: Stereomicroscopic aspects - specimen from set P1 (a) in the flow zone and (b) in the rupture zone; (c) the appearance of an experimental specimen in set P1

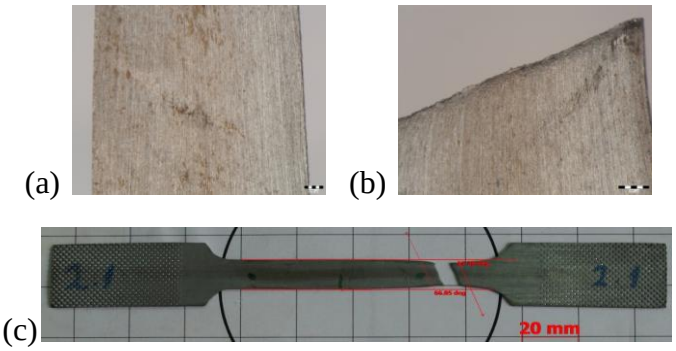

Fig. 5.22: Stereomicroscopic aspects - specimen from set P1 (a) in the flow zone and (b) in the rupture zone; (c) the appearance of an experimental specimen in set P2

The heated samples also show irregular stresses and deformations along the length of the sample, as seen in figures 5.23 (a) and 5.24 (a). In figures 4.36 (a) and 4.37 (b) details of the breaking area of the samples where uneven flow can be observed, the heated regions show a much more pronounced deformation.

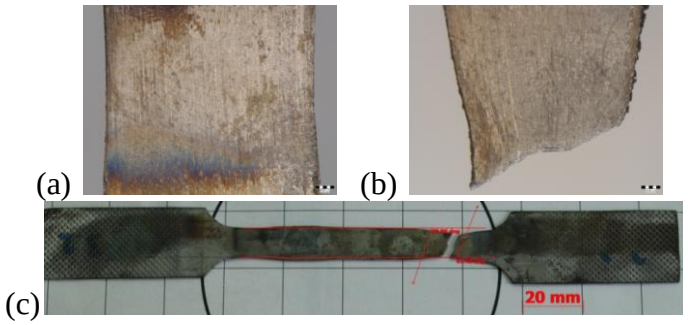

Fig. 5.23: Stereomicroscopic aspects - specimen from set P1 (a) in the flow zone and (b) in the rupture zone; (c) the appearance of an experimental specimen in set P3

Flame heating further observes the anisotropy of properties while the use of induction heating annihilates this anisotropy (Fig. 5. 23). By creating locally heated zones, deformation states are strongly modified in these regions and, because of them, become areas prone to severe deformations (a phenomenon similar to that of voltage concentrators).

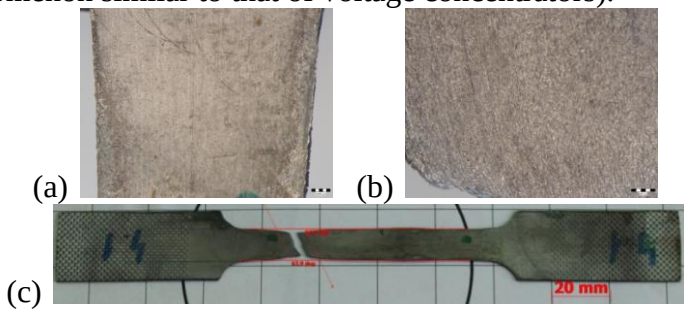

Fig. 5.24: Stereomicroscopic aspects - specimen from set P1 (a) in the flow zone and (b) in the rupture zone; (c) the appearance of an experimental specimen in set P4

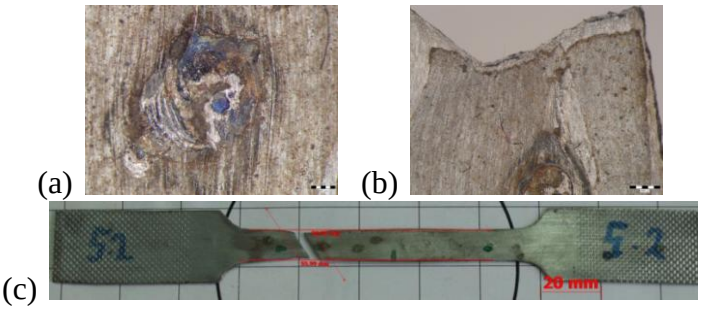

Fig. 5.25: Stereomicroscopic aspects - specimen from set P1 (a) in the flow zone and (b) in the rupture zone; (c) the appearance of an experimental specimen in set P5

In the case of straightening using the spotter method the welding points applied to the material become tension concentrators, the flow of the material in that region becomes uneven, as seen in Figure 5. 25 (a) and the rupture will most likely occur in the vicinity of these regions, the breaking zone indicated in Figure 5. 25 (b) supports that assumption.

Deformation occurs locally, unevenly, which strongly influences the characteristics of ductility, elongation at breakage and strictness decrease compared to a material with a homogeneous state of tension and deformation.

The mechanical characteristics resulting from the straightening in which this method is used are inferior due to different mechanical behaviour due to structural non-homogeneities that become tension concentrators due to strongly different mechanical characteristics.

5.4.3. Determination of compressive strength

From each of the 5 experimental samples, 3 samples were taken which were tested for compression using the RAE method and the specially designed fastening system.

Force-displacement coordinate curves, obtained from mechanical compression tests, are shown in fig. 5. 26.

Analyzing the appearance of the curves presented, a similar aspect is found, a linear variation until a maximum value is reached followed by a gradual decrease and stabilisation at a level. The behaviour of the samples during the test suggests taking a request in the linear-elastic field to the maximum point, the test tube fails by bending due to the very large length/width ratio, then warping the plastic in bending.

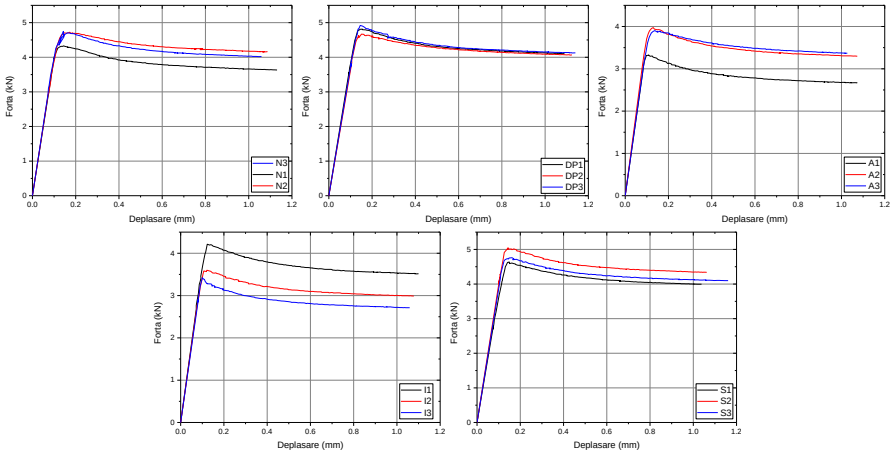

Fig. 5.26: Curves in force coordinates - displacement obtained by compression testing of samples

Processing the experimental curves, the following parameters were extracted: maximum force (Fmax), displacement below the maximum force (Move to Fmax) and the rigidity was estimated to report the maximum force at the corresponding displacement.

Analyzing the average maximum force values, the comparison being shown in Figure 5. 27 (a), close values are found between the samples in set P1, P2 and P3, while the samples in the P4 and P5 set have similar values between them but lower than the ones.

Movements below maximum force, illustrated for comparison in Figure 5. 27 (b), has similar values for p1, P2 and P3 samples, and P4 and P5 samples have similar but lower values.

The rigidity of the metal body elements can be analysed for comparison in Figure 5. 27 (c), where similar results are observed in value, with samples having a stiffness of around 30kN/mm.

In the case of compression application, the non-homogeneous structural state of the test tube does not influence the mechanical characteristics of the material so strongly.

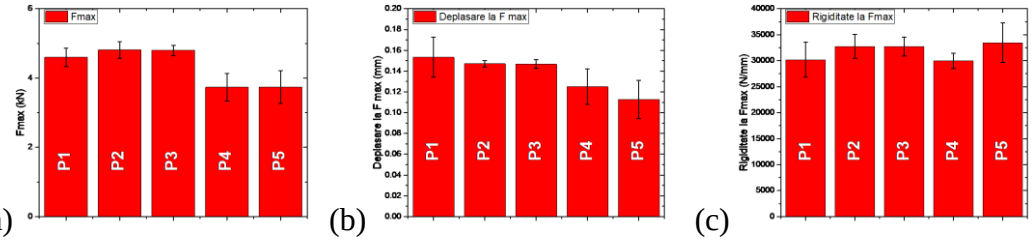

(a) (b) (c)

Fig. 5.27: Comparisons between maximum force values (a), maximum force displacement (b) and stiffness at maximum force for test specimens (c)

5.4.4. Determination of bending strength

For this test, 5 samples were used for each set which were measured using a digital screw with a resolution of 0.01 mm.

The force-movement curves have been processed to obtain the bending elasticity module and a yield strength of 0.2% using the same procedure used to determine the conventional yield strength.

Figure 5. 28 are presented the mediated curves of the 5 samples tested for bending.

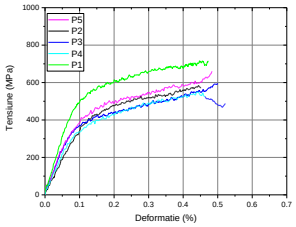

Fig. 5.28: Mediated strain-stress curves for experimental samples

Since the boards have a ductile behaviour, the plastic is significantly deformed, as seen in the figure above, the criterion for assessing the bending resistance was chosen as the yield strength for a deformation of 0.2% determined by a procedure similar to that of the determination of the conventional yield strength.

At the same time, the value of the bending elasticity module was calculated, the average values being used in comparisons. Bend resistance values illustrated for comparison in Figure 5. 29 (a) and shows a drastic decrease for samples directed from the reference ones (taken from the original car panel). However, regardless of the method applied, there are no large differences between values.

With regard to the values of the elasticitemodule tein bending illustrated for comparison in Figure 5. 29 (b) a decrease from the maximum value identified in the P1 samples of the values of the other samples can be observed, the lowest value being observed in the case of P2 samples. Mechanical behaviour during requests is subject to the non-homogeneous structure of the material - the observations and conclusions presented in the traction test shall be valid in the case of this test. Traction and compression components appear in the test tube in the case of bending application. Since a lower influence of the non-homogeneity of the material in compression has been demonstrated, the area subject to traction is predominantly responsible for the mechanical behaviour of the material.

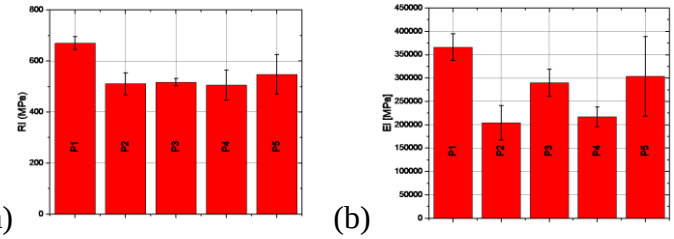

(a) (b)

Fig. 5.29: Comparisons between the mean bending resistance values and the bending elasticity module

5.4.5. Conclusions regarding the mechanical behavior of the material

The determination of Vickers microdurity found an increase in the microdurity values which was considered to be produced by direct plastic deformations, in the case of impact straightening, or indirect, of dilation and contraction products in the case of heated samples.

The traction test highlighted the importance of structural non-homogeneity in the test tube on mechanical behaviour and mechanical characteristics. A control of the parameters of the heating straightening procedure improved the mechanical characteristics resulting from the samples directed by this method, and the study carried out on the samples directed using the spotter method made it possible to identify the mode of failure: the concentration of voltages in the welding thrushes and the rupture of the test tube in their vicinity.

Compression behaviour is little influenced by structural non-homogeneity, the values obtained being similar for all samples.

As regards bending behaviour, in view of the mixed application mode, a variation similar to that observed at compression in the light of the yield strength was found, making it possible to extrapolate observations on mechanical traction and bending behaviour.

Mixed requests arising in the event of an accident require such a study to be able to establish broadly reference values for estimating the mechanical characteristics of remedied experimental samples usable in carrying out safety and impact calculations.

Although all methods lead to mechanical behaviour impossible to predict because of the affected area and the straightening procedure applied, improvement of characteristics is possible by applying strict straightening procedures.

Of all the straightening methods investigated in this study, cold plastic deformation straightening has the best characteristics and would be recommended, but due to the impossibility of application in any situation, the association with other methods becomes necessary and the establishment of a control over the procedure applied proves beneficial.

5.5. Corrosion resistance evaluation

5.5.1. Determination of corrosion resistance by electrochemical method

The corrosion resistance was assessed using the technique of linear polarization (Taffel technique), which consists of tracing polarization curves by measuring the open circuit potential for 1h and tracing linear polarization curves from -250 to 250mV with a scanning speed of 1mV/s.

Several samples from all 5 types of experimental samples (P1, P2, P3, P4, P5) were tested, summarised in Figure 5. 30, the testing of the sample closest to the average of the results obtained corresponding to each type of sample shall be selected for presentation.

The corrosion resistance tests were carried out in accordance with the specifications of the ASTM G5-94(2011) standard, using a Potiostat/Galvanostat APPARATUS 4000, Princeton Applied Research, an electrochemical cell consisting of a reference electrode (calomel saturated electrode), recording electrode (plastin electrode) and working electrode (samples investigated). Testing was performed in a Solution of NaCl with 3.5% concentration.

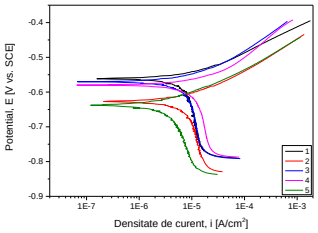

Fig. 5.30: Potentiodynamic curves for all samples investigated (P1, P2, P3, P4, P5)

Using Tafel curves, determining parameters such as open circuit potential (Eoc), corrosion potential ($E_{chorus)}$,corrosion current density ($i_{chorus)}$and slopes of cathode and anode curves (β_c and $\beta_{a)}$waspossible. The results obtained are presented in Table 5.13.

Tabelul 5.1: The main parameters of the corrosion process

Nr. crt.	Proba	Eoc (mV)	Ecor (mV)	i_{cor} ($\mu A/cm^2$)	β_c (mV)	β_a (mV)	Rp ($k\Omega xcm^2$)	CR (µm/an)
1	P1	-593	-561	7,369	620,52	55,67	3,01	85,60
2	P2	-631	-627	8,437	753,64	69,40	3,27	98,01
3	P3	-593	-570	9,05	958,72	73,12	3,26	105,12
4	P4	-594	-580	12,884	865,65	73,81	2,29	149,67
5	P5	-634	-637	4,078	415,89	74,32	6,72	47,37

For easier interpretation, the data in Table 5.12 were represented in the form of bar graphs shown in Figure 5. 31.

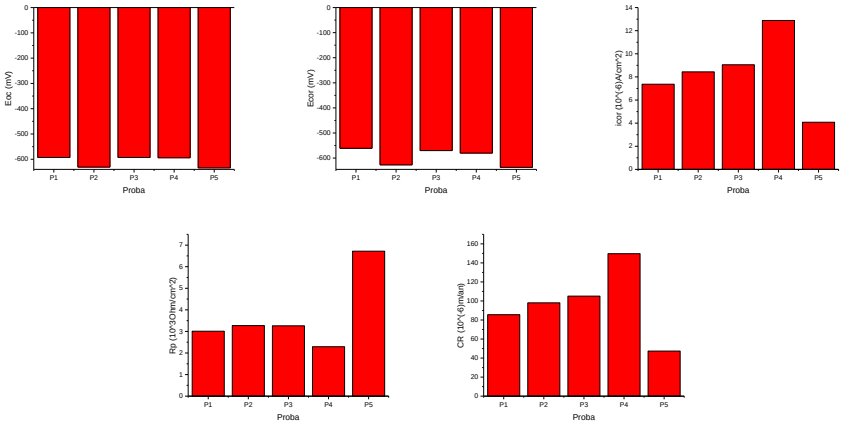

Fig. 5.31: Comparisons between corrosion parameter values: (a) open circuit potential, (b) corrosion potential, (c) the intensity of the corrosion current, (d) polarization resistance, (e) corrosion speed

If we take into account the value of the open circuit potential (E_{oc}) (Fig. 5. 31 a.), it is considered that the more electropositive values denote a more noble character from the electrochemical point of view of the samples analysed, but also a better corrosion behaviour.

Electrochemical measurements, in terms of the evolution of open-circuit potential, showed that samples P1, P3 and P4 recorded the most electropositive values and consequently a more noble character from an electrochemical point of view.

If we take into account the value of corrosion potential (E_{chorus}) (Fig. 5. 31 b.), the values of the corrosion potential E_{chorus} more electropositive are considered to be better underted by corrosion.

From this point of view it is observed that the P1 sample has the most electropositive value of E_{choir} (-561 mV) followed by a difference of only 7 mV of the P3 sample with a value of -570 mV.

It is known that a low corrosion current density (i_{chorus})indicates good corrosion resistance. Thus, if we take this criterion into account, in Figure 5. 31 c. it is observed that the P5 sample has the lowest value of i_{chorus} (4,078 $\mu A/cm^2$)thus demonstrating better resistance than the other samples investigated in terms of corrosion resistance.

It is known that a high polarization resistance highlights a good corrosion behavior of a material, and a small value of this parameter a worse behavior to corrosion. In this case, the highest value is that of the P5 sample (6.72 kρxcm^2).

After calculating the corrosion rate of the samples tested from electrochemical tests carried out in solution 3,5% NaCl, it is observed that the smallest value is obtained in the case of the P5 sample with a value of 47,37 μm/year.

In conclusion it can be said that the P5 sample has superior electrochemical values (the lowest corrosion current density, the highest polarization resistance and the lowest corrosion rate) and thus a better corrosion behavior in solution 3,5% NaCl than all other samples investigated.

5.5.2. Investigation of surfaces affected by corrosion by stereomicroscopy

The investigation of corroded surfaces was carried out using the Olympus SZX7 stereomicroscope to observe the distribution of corrosion asspots.

Figure 5.32 shows the corrosion aspects identified on the surface of sample P1. The formation of a compound is observed in the region in the SV area of the sample in Figure 5.32 (a), the detailed appearance being shown in Figure 5.32 (b). In this area it can be said the existence of a uniform corrosion with the formation of an oxidic compound, of reddish-magnitude, and the appearance of aspects that can be assessed as crevices, evenly distributed in the corroded surface.

(a) 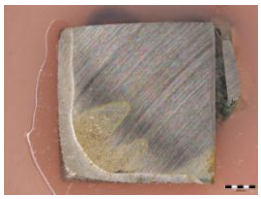 (b) 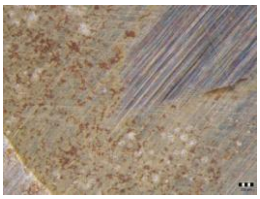

Fig. 5.32: Stereomicroscopic aspects on the surface of the P1 sample after corrosion testing

Figure 5.33 The aspects of corrosion of the surface of the P2 sample are presented. Uniform corrosion can be claimed, the entire surface is affected, but with different degree of damage..

(a) 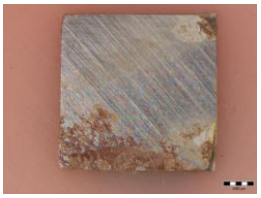 (b) 

Fig. 5.33: Stereomicroscopic aspects on the surface of the P2 sample after corrosion testing

Figure 5. 33 (a) the southern region is more severely affected by corrosion, in this area the effects of cold plastic deformation (cold straightening) are visible by a more intense corrosion of the material, while also observing a gradient in the sense of improving the degree of deformation. Details presented in fig. 5. 33 (b) indicates the appearance of a reddish oxide compound, the affected region, over time, tends towards a crevice corrosion.

(a) 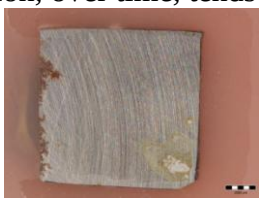 (b) 

Fig. 5.34: Stereomicroscopic aspects on the surface of the P3 sample after corrosion testing

By studying the corrosion aspects observed in the case of sample P3, it can be found in fig. 5. 34 (a), a corrosion located in two regions, with the formation of a reddish colour oxide and a yellow compound (precipitated). Detail shown in fig. 5. 34 (b) suggests uniform corrosion, the surface being uniformly affected, and over time the degree of destruction is prevented to propagate evenly over the surface. By heating and cooling the change in the states of tension and deformation of the material can lead to a localized corrosion.

(a) 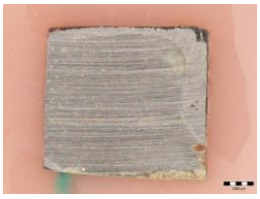 (b) 

Fig. 5.35: Stereomicroscopic aspects on the surface of the P4 sample after corrosion testing

Figure 5.35 The corrosion aspects observed in the P4 sample which is represented by a hot-directed sample using the inductor as a heating source are presented. Compared to the P3 sample, it can be observed that the area affected by corrosion is considerably smaller, being limited to the marginal regions of the sample. In areas affected by corrosion can be seen in Figure 5.35 (b), the formation of a reddish oxide compound.

In the case of sample P5, in fig. 5.36 (a) localised corrosion may be found in the northern and southern regions of the sample. The appearance of the gradient may suggest a differentiated attack between two consecutive welding sores, the structure being affected regionally by cold plastic heating and deformation. In fig. 5.36 (b) a detail of the region affected by corrosion is observed in which a reddish oxide compound along the boundary of a region where a yellow compound/precipitate has formed is observed.

(a) 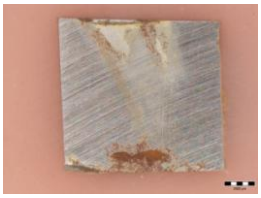 (b) 

Fig. 5.37: Stereomicroscopic aspects on the surface of the P5 sample after corrosion testing

By studying the areas affected by corrosion, a considerably smaller area fraction was assessed in the case of heated-directed samples, while the areas most affected are those directed by cold plastic deformation and the use of spotter.

5.5.3. Investigation of surfaces affected by corrosion by scanning electron microscopy (SEM)

The morphology of the corroded surfaces was inspected using a Phenom ProX, Phenom World-type stalot.

Following the investigation of the surface of the P1 sample after the corrosion test, a selection of micrographs shown in Figure 5 was carried out. 38 from different regions of the sample and at different increases. In these micrographs one can observe a degradation of steel predominant in the region of non-metallic inclusions and scratches induced at the stage of preparation of samples. The preferentially attacked regions can be observed during the corrosion process, suggestive details being found in Figure 5. 38 (a).

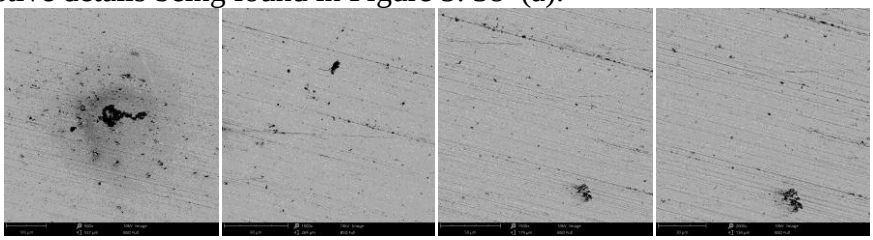

(a) 500X (b) 1000X (c) 1500X (d) 2000X

Fig. 5.38: SEM micrographs obtained from the investigation of the surface of the P1 sample following the corrosion test

In the case of sample P2, the cold-deformed plastic sample, the SEM micrographs obtained on the surface of the corrosion-tested sample are shown in fig. 4. 39. Similar to the appearance of sample P1, an attack located mainly in the region of non-metallic steel inclusions and scratches induced during the preparation of the sample can be observed. The film observed by the analysis using the stereo-microscope was not observed even when investigating the current sample.

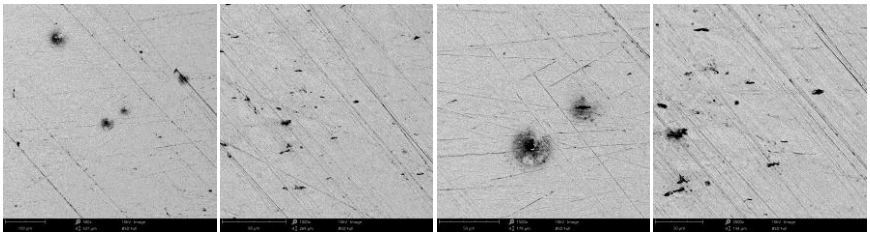

(a) 500X (b) 1000X (c) 1500X (d) 2000X

Fig. 5.39: SEM micrographs obtained from the investigation of the surface of the P2 sample following the corrosion test

The investigation of the tested surface corrosion of the P3 sample led to the obtaining of the SEM micrographs shown in Figure 5. 40. A localized attack is observed mainly in the region of non-metallic inclusions in the material, but the intensity of the corrosion phenomenon is considerably lower than in the case of the P2 sample

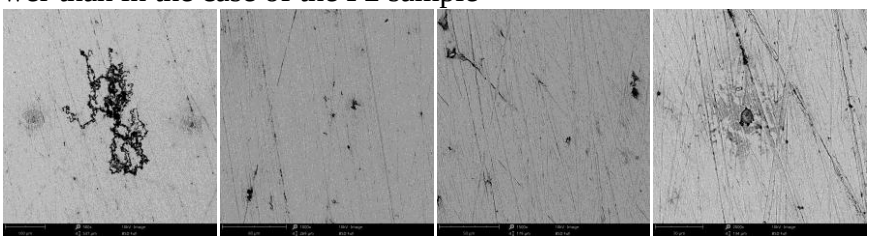

(a) 500X (b) 1000X (c) 1500X (d) 2000X

Fig. 5.40: SEM micrographs obtained from the investigation of the surface of the P3 sample following the corrosion test

By investigating the surface of the P4 sample tested for corrosion obtained from the directed panel using induction as a source, the selected micrographs from different regions are shown in Figure 5. 41 where, similarly, a sharp corrosion occurs mainly in the region adjacent to non-metallic inclusions in the material. Comparing the intensity of these processes and the affected area, it can be assessed that this sample has shown the least degradation.

In the case of the P5 sample obtained from the spotter-directed panel, the SEM micrographs shown in Figure 5were obtained following the surfaceinvestigation. 42 In a first assessment it can be observed that this sample shows the area most extensive surface affected by corrosion, with crevices of irregular shape, evenly distributed throughout the surface. There may also be a sharp degradation of materials in the region of non-metallic steel inclusions.

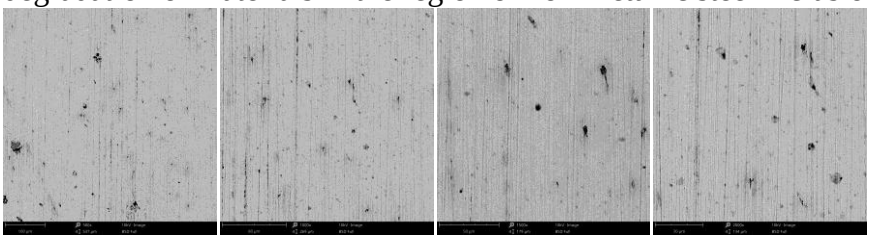

(a) 500X (b) 1000X (c) 1500X (d) 2000X

Fig.5.41: SEM micrographs obtained from the investigation of the surface of the P4 sample following the corrosion test

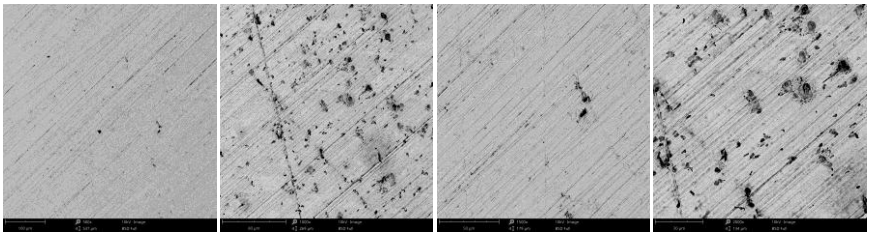

(a) 500X (b) 1000X (c) 1500X (d) 2000X

Fig. 5.42: SEM micrographs obtained from the investigation of the surface of the P5 sample following the corrosion test

Observations made using the scanning electron microscope complement and confirm those made using the stereomicroscope: the most affected surface is that of the P5 sample directed by the "spotter" method. The P2 test, directed by impact, also has a higher intensity of

degradation than the reference sample P1. The least affected are the surfaces of the P3 and P4 samples, directed by heating, which show the lowest intensity of the corrosion process at the surface level.

5.5.4. Conclusions of the corrosion resistance study

In view of the intensity of the corrosion current, the resistance to polarization and the rate of corrosion, the P5 sample exhibits the best behaviour, followed by samples P1, P2, P3 and P4. According to the analysis of open circuit and corrosion potentials indicate the best corrosion behavior of the P1 sample, followed by P3, P4, P2 and P5.

The difficulty in assessing corrosion behaviour through the prism of parameters is induced by the inhomogeneity of the states of tension and deformation in the sample. To complete these observations it was decided to investigate the surfaces affected by corrosion using the stereomicroscope and electron microscope through the sweep. Following the use of the stereo-microscope, the surface of the P4 sample was found to be least affected by corrosion, followed by sample P3, P1, P2 and P5. This hierarchy is closer to expectations based on theoretical concepts: by heating above a certain temperature the state of tension in the material is annihilated (p4 and P3 samples), while the increase in ecruisation (sample P2) leads to an increase in the susceptibility to corrosion to the original state (sample P1). Creating contact between two materials with different electro-chemical characteristics (anchor welded by the spotter method and steel from the car body element) creates galvanic piles and reduced dimensional areas with different voltage stresses and deformations, produced due to heating/cooling.

Studies by scanning electron microscopy by streak confirm, to a large extent, these assumptions: samples P4 and P3 have the lowest intensity of corrosive attack, observed especially in the region of non-metallic inclusions.

The change in the voltage and deformation states of the material by local emphasis of ecruisation (sample P2) accentuates the corrosion process compared to the initial state (sample P1). Righting by using the "spotter" produces the best corrosion behavior because the thermally impaired area is extremely low, the concentration of voltages is carried out only in the region of welding thrush, and as long as there are no favorable environmental conditions for corrosion (humidity), the corrosion process will proceed much more slowly.

5.6. Surface wettability study

After measuring the contact angle, following an analysis of the distribution of the values, it was decided to group them into three regions, then the superficial energy of the material was calculated for each sample.

Following grouping according to values, the results obtained are presented, in the form of a bar graph, in Figure 5.43.

The distribution of contact angles when water has been used as liquid can be observed in Figure 5.43 (a) where, regardless of the region studied, the values of the angles are similar for samples P1, P2 and P3, except in the case of region R1 of sample P3 (P3-R1), the determination being made on a welding afta. In the case of heat-directed samples, P3 and P4, a decrease in contact angle values and a strong variation in the heat gradient case at heating are observed. The surface becomes more hydrophile, is better watered, and, inherently, more prone to corrosion. The use of ethylene glycol (Fig. 5.43 (b)) and diiodomethane (Fig. 5.43 c.) has similar contact

angle values in the case of higher P1 and P5 samples, with P2, P3 and P4 being in the same value region.

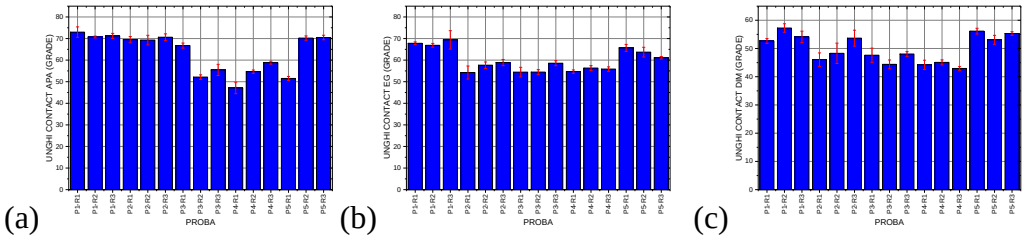

(a) (b) (c)

Fig. 5.43: Average contact angle values in the three regions (R1, R2, R3) for liquids used: (a) water, (b) ethylene glycol (EG) and (c) diiodomethane (DIM)

Due to the different characteristics of the liquids used (polar and dispersive components of energies) associated with the energy characteristics of the surface (also polar and dispersive components) the variation in the values of the contact angles can be attributed to the dominance of either the polar or the dispersive components.

Following the calculation of free surface energy using the theoretical method and the Fowkes method the results are presented in figu5.44 in the form of a bar graph.

Analyzing the variation in theoretically estimated free-energy area, there is a gradual increase in value in order P1, P2, P3, P4 and P5.

In the case of P1 and P2 samples, no strong variation is found, the values being quite close and lower than the P3, P4 and P5 samples which also have close values.

Using the Fowkes method a similar variation is observed, samples P1 and P2 exhibit close, lower than P3 and P4, which are also quite close.

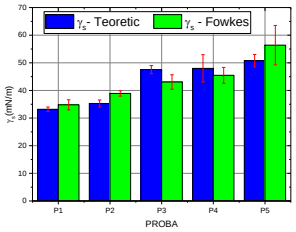

Fig. 5.44: Comparisons between the surface free energy values of the solid

Analyzing the variation in theoretically estimated free-energy area, there is a gradual increase in value in order P1, P2, P3, P4 and P5.

In the case of P1 and P2 samples, no strong variation is found, the values being quite close and lower than the P3, P4 and P5 samples which also have close values.

Using the Fowkes method a similar variation is observed, samples P1 and P2 exhibit close, lower than P3 and P4, which are also quite close.

The highest value of free energy can be observed in the case of the P5 sample. The discrepancies between theoretical and experimental values are relatively small in the case of P1 and P2 samples, the structural condition of the material does not change strongly, nor, inherently, in the condition of the surface of the material.

Significant discrepancies begin to occur in P3, P4 and P5 samples, where different surface straightening methods affect the flatness and deviation from an ideal surface (various phases present on the surface, roughness inducing) that could be corrected using methods found in the literature such as the models proposed by Wenzel and Cissie-Baxter. The application of these models implies an extensive characterization of the surfaces which comes out of the direction of the request addressed in the present paper.

Although heating and cooling in the air is expected to achieve a structure closer to equilibrium which would result in a lower surface energy, the conditions under which heating was carried out (by region, uneven) induce different states of deformation and tension in the material, a consequence of uneven dilation and contraction in the material, which largely explains the increase in the value of superficial energy.

The results obtained in this study indicate that the cold plastic deformation –P2 sample has the closest contact angle and surface free energy values to those of the reference sample P1, therefore a similar wetability behaviour is assessed which is reflected in the corrosion resistance of the alloy. For these reasons, it was concluded from this analysis that the most appropriate method of straightening the experimental samples is cold plastic deformation.

CHAPTER 6: IMPROVING THE CORROSION RESISTANCE OF EXPERIMENTAL SAMPLES BY COATING WITH ALUMINA USING PLASMA SPRAYING DEPOSITION

6.1. Alumina coating of experimental samples by thermal spraying

The samples obtained were characterized by optical and electron microscopy and corrosion resistance was determined. The coding of the samples was maintained according to previous studies and the letter "A" was added before the default indices, as can be seen in the following table.

Tabelul 6.1: Codificarea eșantioanelor experimentale acoperite

Codificare	Procedură de îndreptare
AP1	Probă de referință acoperită(prelevată din panoul original)
AP2	Probă deformată plastic la rece și acoperită
AP3	Probă îndreptată prin încălzire cu flacără și acoperită
AP4	Probă îndreptată prin încălzire cu inductor și acoperită
AP5	Probă îndreptată prin metoda "spotter" și acoperită

6.2. Optical microscopy analysis of the deposited layer

In order to determine the thickness of the layer and how it adheres to the substrate, coated samples were prepared metalographic in longitudinal section. Figure 6.1 shows the optical micrographs obtained in different regions of the sample.

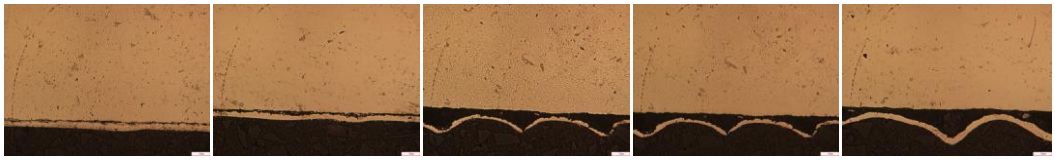

AP1 AP2 AP3 AP4 AP5

Fig. 6.1: Optical micrographs showing the substrate, interface and layer deposited for experimental samples

By inspecting the micrographs obtained for the AP1 sample, a layer of approximately uniform thickness, relatively adhering to the surface, but showing discontinuities in the shape of pores, is found. The layer deposited on the AP2 sample also has a relatively uniform thickness in

some regions. Its adhesion is lower than the layer deposited on the AP1 sample, showing areas where obvious exfoliation occurs. The layer deposited on the AP3 sample is relatively uniform in thickness, but its adhesion can be assessed as inferior due to exfoliation. The layer deposited on the AP4 sample has an uneven thickness and almost complete exfoliation, a similar aspect observed in the AP5 sample. The layers deposited on the heat-directed samples show exfoliations indicating a poor adhesion to the substrate, and their thickness is variable and significantly lower than those directed without heating.

Appreciating the mean value of the layer thickness, it is found that samples that had a substrate that was not subjected to heating (AP1, AP2 and AP5) have considerably higher thicknesses than those of samples whose substrate has been heated (AP3 and AP4). The change in layer thickness over the length investigated is reduced in the case of AP2 (7.86μm), while in the case of the AP1 sample the change in thickness is slightly higher (12.86 μm). The AP3 sample has a thickness variation interval of 13.55 μm and the AP4 sample of 18.70 μm. The highest value of the range of variation was observed in the AP5 sample (21.01 μm). The thickness of the layer appears to be influenced by the way the substrate is processed in this heating temperature study.

6.3. Scanning electron microscopy (SEM) and energy dispersive X-ray spectroscopy (EDS) analysis of the deposited layer

All the coated samples were investigated, but since the morphology of the layers was similar, a selection of micrographs obtained by investigating the AP1 sample was chosen in the paper.

The deposited layer is discontinuous, pores and gaps are observed, making it easy to identify "splash"-looking formations resulting from the deposition mode. At large magnifications (Fig. 6.2 (c) and (d)) microcracks can be observed in the deposited layer, as well as the gaps and pores present.

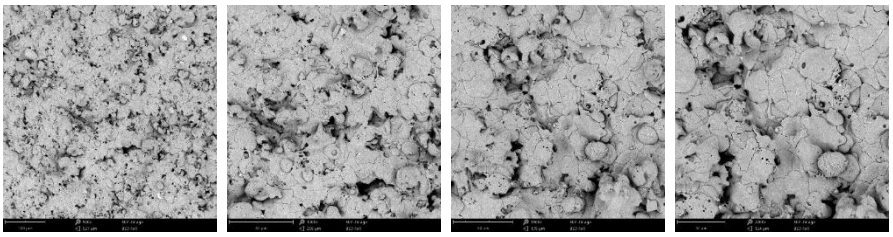

(a) 500X (b) 1000X (c) 1500X (d) 2000X

Fig. 6.2: SEM micrographs showing the morphology of the AP1 sample layer

Figure 6.3 shows a SEM image (at 3000X magnification) representative of the surface of the AP1 sample, on which the EDS analysis was carried out, an image representing the map of the distribution of the constituents found in the coated area of the sample and their distribution, as well as the constituent graph showing their distribution and concentration. Thus, according to the results, the majority presence of aluminium and oxygen indicates the presence of a coating of Al_2O_3 on the surface of samples of a steel of the group of non-alloyed quality steels.

(a) 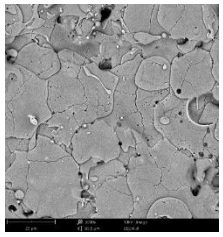 (b) 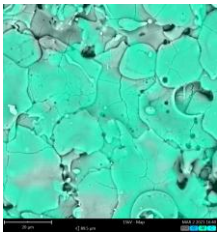 (c) 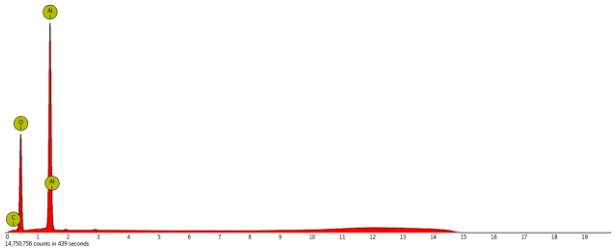

Fig. 6.3: The results of the SEM and EDS analysis for the representative AP1 sample: (a) SEM micrography of the area on which the EDS analysis was carried out; (b) the map of the constituents and their distribution; (c) the graph of the distribution of the elements

6.4. X-ray diffraction analysis of the deposited layer

From the analysis of the results by comparison, it can be observed that the undistorted base material has a structure made up of ferrite, and after coating it can be observed the presence of the compound Al_2O_3 (alumina) with which it was coated.

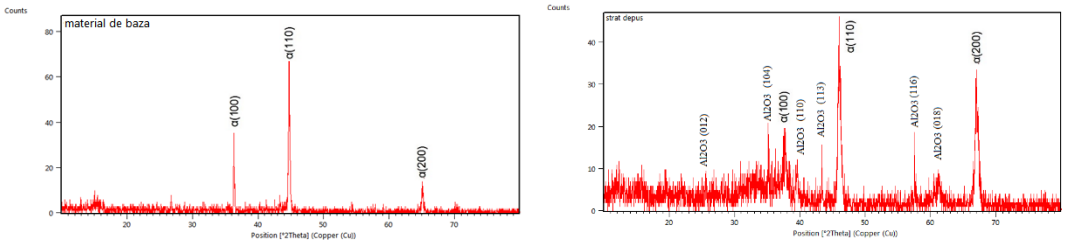

(a) Sample P1 *(b) Sample AP1*

Fig. 6.4: Comparison of difractograms of initial samples: a) before coating and b) after coating

From X-ray diffraction analyses, the presence of the following compounds in the experimental samples can be observed:

- Base Material – Ferite
- Coated– Ferit and alumina.

6.5. Determination of the bending strength of coated samples

The 3-point bending test was performed under conditions similar to that performed for uncoated samples: the ASTM D790-17 standard test guide was used using the Walter+Bai LFV300 universal test machine equipped with the 3-point bending device that complies with the asTM C393, ASTM C1161 and ASTM D790 standard specifications.

The distance between the reasemes was 60 mm, the diameter of the rollers used for the reazem and for the one applying the request was 25 mm, and the test was carried out at a speed of travel of 1 mm/min.

The test tube has been positioned in the device so that the roll applying the request makes contact with the uncoated portion of the test tube.

For each state, 5 samples were tested, the resulting voltage-deformation curves were mediated and the yield strength of 0,2 % was used as a failure criterion, a procedure similar to that used in the testing of uncoated samples.

Figure 6.5 shows, comparatively, the voltage-deformation curves for coated samples (AP) and uncoated (P) curves in the investigated states.

Through a visual analysis of the curves in the figure above it can find a general behavior similar to the bending of coated and uncoated samples: a significant plastic deformation suggesting ductile behavior.

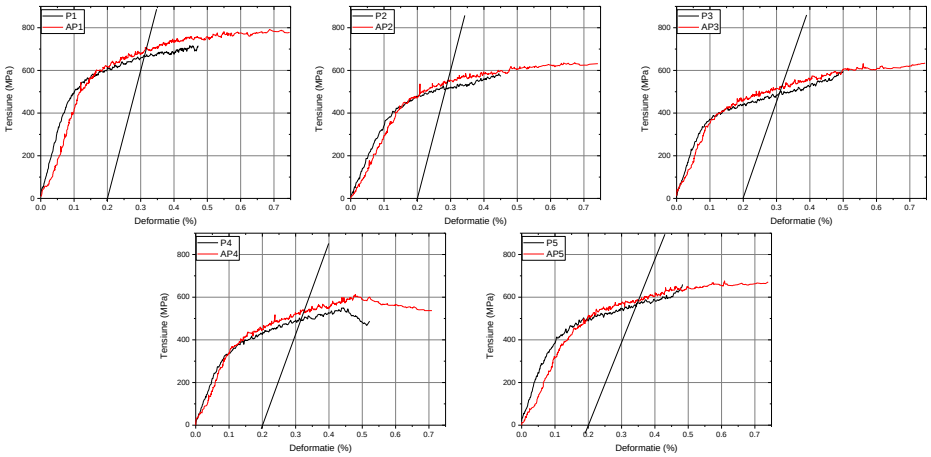

Fig. 6.5: Comparison between voltage-deformation curves determined by the bending test for experimental samples, comparing coated samples (AP) with uncoated ones (P)

Analyzing the starting portion of the curve, in the field of linear - elastic behavior, we find a transition region in which the curve changes its slope by oscillation and a slight translation to the right of the curve. By identifying these points on the voltage-bending curves, the value of the voltage at which the layer gives way was assessed, the variation being shown in Figure 6.6 for each set of samples.

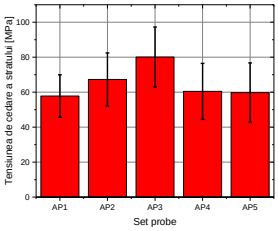

Fig. 6.6: Variation in voltage at which the layer breaks

By inspecting the variation shown in Figure 6.7, the AP3 sample set is found to have the highest value, followed by the AP2 set. The AP1, AP4, and AP5 sets have close values. In view of the large scattering caused by the non-homogeneous state of voltages and deformations in the test samples and the variable thickness of the layer, a justification for this variation may be induced: in the case of ap2 samples, deformed cold plastic, the area resulting from this procedure is not perfectly flat, which leads to an increase in the thickness of the layer in certain regions, and in the case of AP3 samople , directed with flame, a change in the surface that improves the adhesion of the layer may be assumed, this sample indicating the highest estimated surface free energy value using the Fowkes method.

Investigating the bending resistances of coating samples compared to those of uncoated samples, a slight improvement is seen in Figure 6.8.

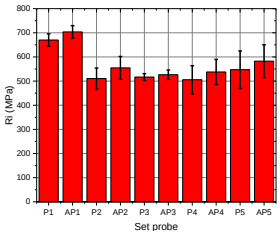

Fig. 6.8: Comparisons between the bending resistances of uncoated and coated

In the case of samples obtained from initial panels, there was an increase in bending resistance of approximately 5%, in the case of those straightened by deformation of approximately 9%, those directed with flame of approximately 2%, those directed by induction and using the spotter method of approximately 6%.

The presence of deposited layers does not bring a statistically significant improvement in mechanical characteristics, but has a good adhesion to the substrate, without exfoliation or cracking over extended regions in the requested region. Since their purpose was to improve corrosion resistance, good adherence contributes to its fulfilment.

6.6. Evaluation of corrosion resistance of coated samples

6.6.1. Determination of corrosion resistance of coated samples

The corrosion test of the coated samples was carried out under the same test conditions as the uncoated samples: the technique of linear polarization was used by tracing the polarization curves by measuring the open circuit potential for 1h and tracing the linear polarization curves from -250 to 250mV with a scanning speed of 1mV/s. The tests were carried out using the same Potentiostat/Galvanostat PARSTAT 4000 in NaCl solution with a concentration of 3.5%. Figure 6.9 (a) shows the potentiodynamic curves obtained from the tests. Figure 6.9 (b) shows the potentiodynamic curves for the samples investigated.

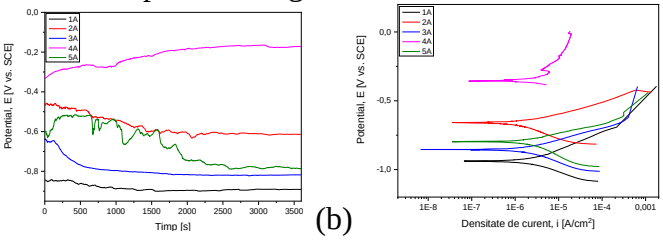

(a) (b)

Evolution of open circuit potential (E_{oc}) over time and Potentiodynamic curves of investigated samples

Using The Tafel curves were determined the parameters uilizate for comparison: open circuit potential (Eoc), corrosion potential (E_{chorus}), corrosioncurrent density (i_{chorus}).

Table 6.2 presents the main parameters of the corrosion process determined by the processing of the experimental results.

Tabelul 6.2: The main parameters of the corrosion process

Proba	E_{oc} (mV)	E_{cor} (mV)	I_{cor} ($\mu A/cm^2$)	βc (mV)	βa (mV)	Rp ($k\Omega x cm^2$)	P	Pe (%)
AP1	-891	-936	2,607	121,12	133,44	10,58	0,3	64,6
AP2	-613	-659	2,618	161,28	89,86	12,97	14,1	68,9
AP3	-817	-854	2,104	121,05	93,94	12,38	0,5	76,7
AP4	-171	-355	3,979	78,88	779,06	7,82	1,9	69,1
AP5	-786	-796	2,055	145,92	77,88	10,74	1,7	49,6

Figure 6.10 shows, comparatively, in the form of a bar graph, the experimental results inidcate in Table 6.2.

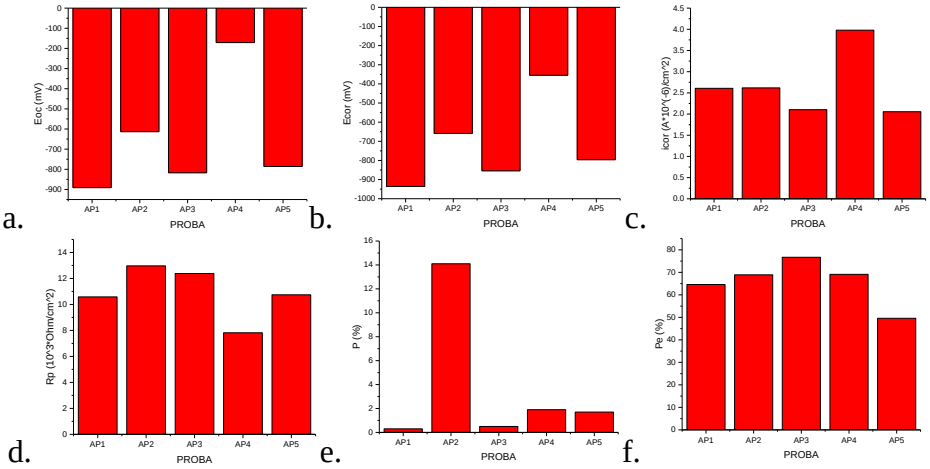

Fig. 6.10: : View of the results obtained from the determination of corrosion parameters indicating comparisons between (a) open circuit potential, (b) corrosion potential, (c) corrosion current, (d) polarization resistance, (e) layer porosity, and (f) protection from corrosive attack

Analyzing the results through the prism of open circuit potential (E_{oc})in Figure 6.10 (a) it is found that the most electropositive values occur in the case of the AP4 sample, followed by the AP2, AP5 and AP1 sample. The more electropositive values of the open circuit potential denote a more noble character from an electrochemical point of view, therefore the AP4 sample shows the best corrosion behavior.

Considering the corrosion potential (E_{cor}) the variation of which is shown in Figure 6.13 (b) is observed a variation identical to that of the open circuit potential, the most electropositive values being observed in the AP4 sample, followed by AP2, AP5 and the last AP1. The more electropositive values of corrosion potential indicate better corrosion behaviour, and based on this parameter the best corrosion behaviour is presented by the AP4 sample.

Studying the variation in the corrosion current density (i_{chorus})shown in Figure 6.10 (c) it is found that the AP3 sample has the lowest values, very close to those of the AP5 sample, and the AP1 and AP2 samples have similar values, but above the AP3 and AP5 samples. The highest corrosion current density value can be observed in the AP3 sample. A lower corrosion current value indicates better corrosion resistance, so we can assess that AP3 and AP5 samples have the best corrosion resistance.

Polarization resistance (Rp) the variation of which is shown in Figure 6.10 (d) has increasing values in the SEQUENCE of the AP4 sample, followed by the AP1, AP5 and AP3 sample, the highest value being observed in the AP2 sample. High-value polarization resistance

suggests better corrosion resistance, and from this parameter it can be assessed that AP2 and AP3 samples have a close resistance.

The assessment of porosity (P) using electrochemical parameters complements the experimental results. The variation of this parameter according to the sample is indicated in Figure 6.10 (e) in which the highest porosity is observed in the AP2 sample, while the lowest porosity is observed in the AP1 sample. The AP3 sample has values close to those of the AP1 sample, while the AP4 and AP5 samples show close and intermediate values to the AP2 and AP3 samples.

By studying the variation of the corrosive attack protection index (Pe) shown in Figure 6.10 (f) the highest value can be found in the AP3 sample, the AP2 and AP4 samples have similar and lower values, and the AP5 sample has the lowest value of this parameter.

Following this test, a contradiction can be found in the results obtained: in the light of the corrosion potentials the AP4 sample would indicate the best corrosion behaviour, while the AP3 sample would behave better only than the AP1 sample, and in the light of the inessiness of the corrosion current and the resistance to polarization the AP3 sample would exhibit the best corrosion behaviour , while the weakest AP4 sample. Conflicting results can be attributed to the non-homogeneity of the deposited layer: porosities, gaps, exfoliations, which mainly affects the accurate and precise estimation of the areas that are reflected on the estimates of some parameters. The attempt to estimate porosity and the corrosive attack protection index does not necessarily present a concrete situation, and in order to obtain additional information it was decided to investigate the surfaces of the corroded samples using microscopy techniques (stereo-microscopy and electron microscopy by sweeping).

6.6.2. Analysis of the surface of the coated samples following the corrosion tests by stereomiscroscopy

Coated and corroded samples were investigated using the Olympus SZX7 stereo-microscope to investigate their surface area for corrosion. Figure 6.11 shows a selection of macrographs recorded during the investigation

AP1 **AP2** **AP3** **AP4** **AP5**

Fig. 6.11: Aspects of surfaces of corrosion-tested samples investigated using stereo-microsc

By studying the surfaces of the samples tested for corrosion using the stereo-microscope on their surface, it was possible to identify the appearance of small reddish compounds, evenly distributed over the entire surface in the case of the AP5 sample, the appearance of a film on the surface of the AP2 sample and large reddish compounds, few in number, in the case of the AP4 sample. In general, the surfaces do not exhibit obvious corrosion degradation aspects which make it possible to make an objective assessment of corrosion behaviour possible

6.6.3. Surface analysis of the surface of the coated samples following the corrosion tests by scanning electron microscopy (SEM)

Since observations of the stereo-microscopy studies were not conclusive, it was chosen to study corroded surfaces using the electron microscope through phenom ProX, Phenom World. The magnification power and the superior contrast facilitate the identification of corrosion products on the surface of the sample.

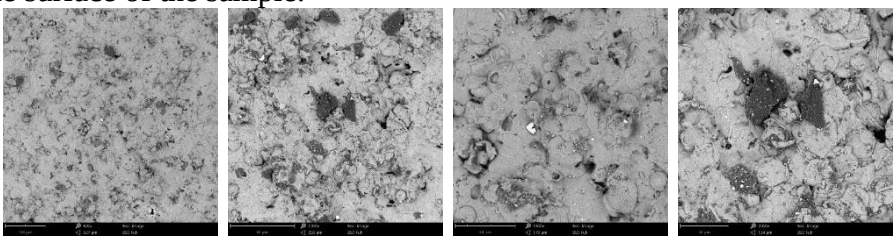

(a) 500X (b) 1000X (c) 1500X (d) 2000X

Fig. 6.12: Micrographs obtained by SEM for AP1 sample

Figure 6.12 shows a selection of micrographs recorded following the investigation of the AP1 sample. Compounds resulting from the corrosion process (Fig. 6.12 (a) and (b)) which appear to be located predominantly in the region of layer discontinuities may be observed on the surface of the sample. These compounds, studied at larger magnifications (Fig. 6.12 (c) and (d)), exhibit a layered morphology, without cohesion between them, but of approximately equal thickness. These compounds are evenly distributed on the surface, covering 14-20% of the investigated surface.

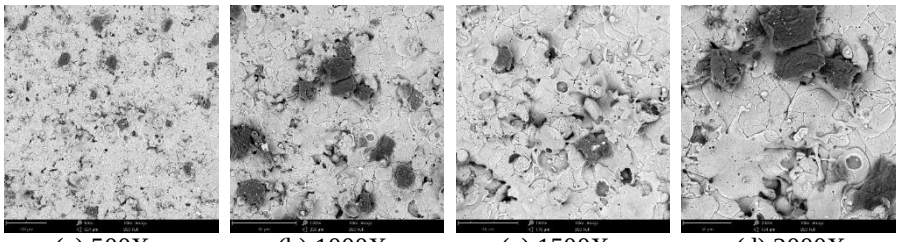

(a) 500X (b) 1000X (c) 1500X (d) 2000X

Fig. 6.12: Micrographs obtained by SEM for AP2 sample

The investigation of the surface of the AP2 sample also observed the existence of compounds of considerably larger size than in the case of the AP1 sample, with a uniform distribution on the surface (Fig. 6.12 (a) and (b)). And in this situation they seem to be located in the proximity of discontinuities in the layer. At large magnifications (Fig. 6.12 (c) and (d)) a similar morphology can be observed, being made of layers, but in this situation the layers show cohesion. In the light of this aspect, a more accelerated corrosion process can be assessed than the AP1 sample. Through accelerated growth and expansion they appear to occupy an area of 20-25% of the area under investigation, a higher share of the AP1 sample.

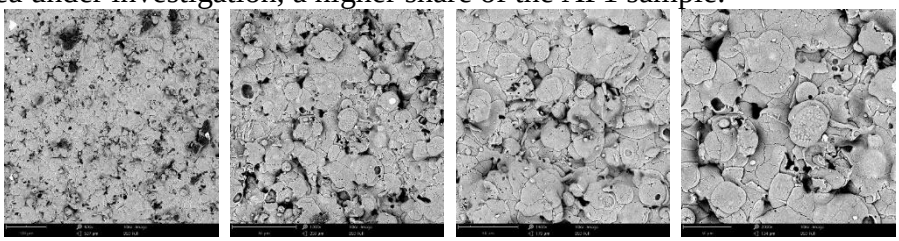

(a) 500X (b) 1000X (c) 1500X (d) 2000X

Fig. 6.13: Micrographs obtained by SEM for AP3 sample

The micrographs obtained by investigating the AP3 sample are shown in Figure 6.13, where the presence of reaction products on the surface can also be found (Fig. 6.13 (a) and (b), but in this situation a preferential orientation can be observed, being linearly arranged and parallel to the direction of the NV-SE.

The study of these compounds at larger magnifications (Fig. 6.13 (c) and (d)) indicates a stratified morphology without cohesion between layers, suggesting a slower corrosion process than the AP2 sample and even AP1, if the thickness and number of layers observed is considered.

Appreciating a proportion of the area affected by corrosion, in the case of this sample, 15-20% of the area under investigation affected by corrosion is approximated.

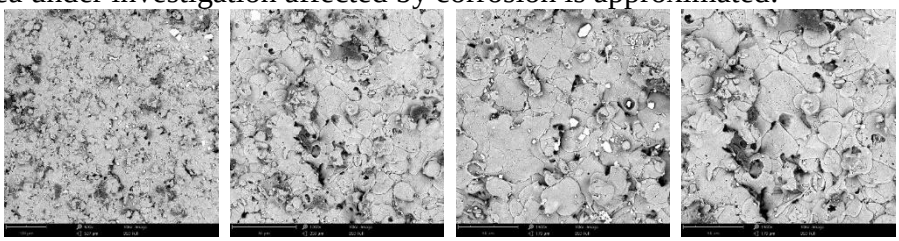

(a) 500X (b) 1000X (c) 1500X (d) 2000

Fig. 6.14: Micrografii Micrographs obtained by SEM for AP4 sample

Studying the micrographs shown in Figure 6.18 obtained by investigating the surface of the AP4 sample, it was also found that there were reaction products of irregular shapes (Fig. 6.14 (a) and (b)) with larger dimensions than those observed in the AP4 sample. They can also be seen in the direction of E-V. The study of these compounds at large magnifications (Fig. 6.14 (c) and (d)) their lamellar morphology is no longer evident, they appear predominantly monoblock, with pores and cracks. Although they have a smaller number on the surface, the upper dimensions have estimated that they occupy 15-20% of the area under investigation.

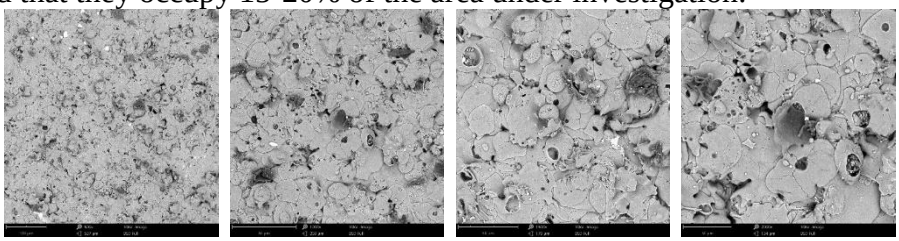

(a) 500X (b) 1000X (c) 1500X (d) 2000X

Fig. 6.15: Micrografii Micrographs obtained by SEM for AP4 sample

Figure 6.15 shows micrographs obtained by investigating the surface of the AP5 sample after corrosion test. Large reaction products (Fig. 6.15 (a) and (b)) were also observed on the surface, located only in certain regions of the surface.

Their morphology, observed at large increases (Fig. 6.15 (c) and (d)) suggests a layered structure, being developed. Appreciating the damage caused by corrosion is estimated a proportion of 15-20% of the area under investigation.

In order to more accurately quantify the surface proportions affected by corrosion, the grid method was implemented to determine these proportions on micrographs obtained at the same magnification. The results of this investigation are shown in Figure 6.16.

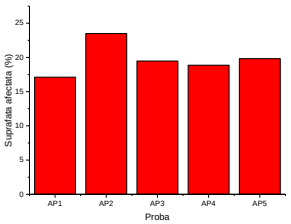

Fig. 6.16: Comparisons between proportions of surface affected by corrosion

Appreciating the results obtained and indicated in Figure 6.16, it is found that sample P1 has the lowest area affected by corrosion, while the highest P2 sample. Samples AP3, AP4 and AP5 have similar and intermediate proportions of AP1 and AP2 samples.

Taking into account the size of the compounds observed on the surface in the AP2 sample, with the largest area affected, the largest dimensions of the reaction products were observed, the decreasing hierarchy of the size of the reaction products being AP4, AP5, AP3 and AP1. By linking the surface percentage with the size of the reaction products, we can assess that in the case of AP2, AP5 and AP3 samples we can consider a more localised corrosion, while in the case of AP4 and AP1 samples a more uniform corrosion can be assessed.

6.7. Comparative evaluation of the efficiency of the coating

parameters determined by processing the curves recorded during the tests was also chosen. Thus a direct comparison was made between the values of open circuit potential and corrosion potential, corrosion current density and plarization resistance. Figure 6.17 shows, comparatively, in the form of a bar graph, the variation of these parameters for the samples coated and uncoated.

The previous study on uncoated samples indicated the best corrosion behaviour of the P5 sample, while that of the P4 sample was considered the weakest.

In the case of coating samples, the best corrosion behaviour in the AP4 and AP3 samples was assessed and the weakest was assigned to the AP1 sample.

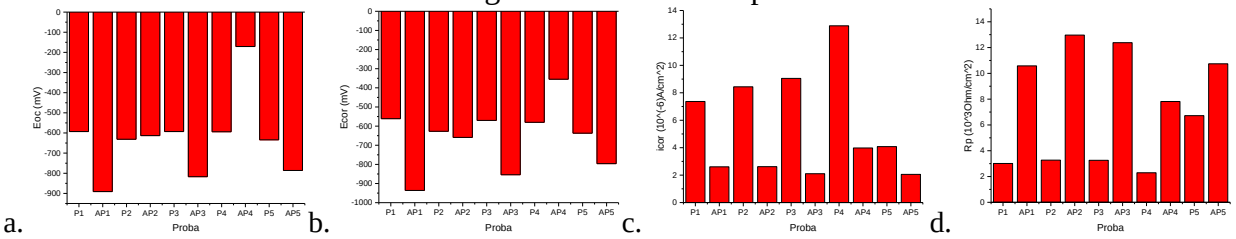

Fig. 6.17: Comparisons between corrosion parameters of uncoated and coated samples illustrating the variation (a) of the open circuit potential, (b) the corrosion potential, (c) the corrosion current density and (d) the polarization resistance

Using as a comparison criterion the value of the open circuit potential, when more electropositive values denote more electrochemically noble, by analysis Figure 6.17 (a) it can be observed that the coating of the sample taken from the original panel leads to worsening corrosion resistance, with AP1 sample indicating values lower than sample P1.

In the case of the cold-hit sample, there is a slight improvement in corrosion behaviour, but further tests are required to justify the efficiency of the process.

In the case of the heat-directed sample using the flame as a heat source, corrosion behaviour is also observed, the value of the open circuit potential of the AP3 sample being more negative than the P3 sample, the uncoated sample.

The most spectacular improvement can be observed in the case of the heat-directed sample using the inductor as a source, where the coating leads to obtaining the most potentially open circuit electropositive. The coating of the sample obtained by straightening using the "spotter" method does not improve corrosion behaviour, with the AP5 sample having a lower value of the open circuit potential.

From the perspective of corrosion potential (Fig. 6.17 (b)), where more electropositive values indicate better corrosion behaviour, a similar variation is observed as with the assessment using the open circuit potential as a criterion: the only improvement in corrosion behaviour by coating can be identified in the case of the heat-directed sample using the inductor.

The corrosion current density, if lower values, reflects better corrosion behaviour can be assessed in Figure 6.17 (c) According to this criterion, significant improvements in corrosion behaviour occur in all samples, but its definition should be taken into account: surface reporting, a parameter difficult to quantify in the case of discontinuous layers and with zonal exfoliation.

A higher value of polarization resistance suggests better corrosion resistance, and the coating of the samples indicate an improvement in the polarisation, as seen in Figure 6.17. Direct comparison can assess an improvement in corrosion behaviour as a result of alumina coating, but in order to justify the process, a service assessment of the efficiency of the coating is required which can justify the additional costs.

GENERAL CONCLUSIONS, ORIGINAL CONTRIBUTIONS AND VALUATION OF RESULTS

C1. GENERAL CONCLUSIONS

This doctoral thesis addressed the metallic materials used in road vehicle body elements, respectively the use of thermo-mechanical processing technologies and plasma jet coatings for the reconditioning and commissioning of metal body elements involved in road accidents that had as consequent deformations of these parts.

Reconditioning deformed metal body elements following collisions is a complex procedure, which includes various aspects. At industrial level, there is no standard unitary procedure to ensure repeatability and reproducibility of results, the succession, choice and application of procedures being left to the staff involved.

In the automotive industry there are several procedures for thermo-mechanical processing of metal body elements deformed as a result of road accidents. Their application induces local structural changes of the steels used in their execution, resulting in a change in the mechanical properties of the body elements. The mechanical behavior becomes different, which involves reducing the safety factor of the car and inducing systematic errors in the case of technical research conducted in road accident expertise.

The aim of this thesis was to evaluate the efficiency of thermo-mechanical processing technologies used for reconditioning deformed metal body elements, by investigating their mechanical characteristics and corrosion resistance, as well as to provide solutions for optimizing these processing technologies.

In order to evaluate the procedures used at the industrial level, an initial study was carried out in which metal body elements from the same manufacturer and the same type of vehicle with relatively similar deformations produced by the collision were analyzed. These corrosion

elements have been directed at the industrial level, using different thermo-mechanical processing technologies: cold plastic deformation (impact straightening) and hot plastic deformation, with two different heating sources, respectively with oxyacetylene flame and by induction. A similar, intact metal body element obtained from the vehicle manufacturer was used for reference. The experimental determinations performed in the initial study aimed to determine the chemical composition of the steel from which the body element is made by spectrochemical methods, microstructural investigations by light microscopy and scanning electron microscopy, evaluation of mechanical properties by Vickers hardness determinations and tensile testing.

The chemical composition of the steel revealed a Werkstoffnummer 1.0389 steel that complies with the specifications of ISO 6317 (2000). Following the experimental researches of optical microscopy, a significant increase of the grain size was found, in the case of the use of hot plastic deformation, the largest grain size being observed in the case of the use of oxyacetylene flame heating. The mechanical characteristics are strongly influenced by this regional variation of the grain size, aspect demonstrated after the tensile test by a variation of the mechanical characteristics. In order to elucidate the variation of the results obtained after the tensile test, a study was carried out that focused on the hardening and local deformations in the specimens that led to the establishment of a model for the mechanical behavior of the specimens in the tensile test. The uncontrolled and local increase of the grain size induces an unpredictable behavior of the material through the presence of structural inhomogeneities and anisotropy that induce uneven states of stresses and deformations in the material. Following the study, it was estimated that the yield strength of steel is the parameter that best describes the tensile test behavior.

Reconditioning of metal body elements that have been involved in road accidents cannot be performed only by cold plastic deformation, due to the geometry or deformations present. For this reason, the use of hot plastic deformation is mandatory and it has been shown that in order to optimize the heating process it is necessary to reduce the phenomenon of increasing the grain size. The heating process parameters were optimized by estimating the critical temperatures of the steel using equations from the literature and an equation that estimates the austenitic grain size as a function of temperature and holding time. The identification of the heating temperature and the maintenance time was made by analyzing and optimizing the equations used, these parameters being transposed by establishing a procedure that was implemented in the workshop that required estimating the critical temperature of steel, evaluating the heating temperature using a table standard colors and shortening of the zonal heating period. The efficiency of the proposed procedure was verified by its implementation at the industrial level, using a new set of metal body elements obtained from the same type of vehicle and from the same manufacturer, with a similar degree of deformation.

Deformed metal body elements have been reconditioned using the following technologies: cold plastic deformation; hot plastic deformation, with heating by oxyacetylene flame; hot plastic deformation with induction heating. Also, the “spotter” method was introduced, according to the industrial name.

The microstructural characterization of steels was performed using optical microscopy and scanning electron microscopy, the determination of mechanical characteristics was performed by

tensile, compression and bending tests, and the corrosion resistance was evaluated by the linear polarization technique.

The results of the corrosion test led to the improvement test by applying an alumina coating, the samples obtained being also evaluated in terms of corrosion behavior.

The steel from which the experimental samples were made were quality non-alloy steels, with a chemical composition that classifies them in class E185 according to ISO630 (1995).

Experimental research in optical microscopy and scanning electron microscopy has shown a predominantly ferritic structure, with inclusions of globular-shaped oxides and sulfides. Experimental research on grain size did not show a significant increase, thus demonstrating the effectiveness of the procedure implemented for hot plastic deformation.

The mechanical tests performed experimentally were: tensile test in accordance with the provisions of ISO 6892, compression test and bending test guided by the ASTM D790-17 standard. The results of the mechanical tests revealed a strongly different mechanical behavior in the case of tensile stresses caused by structural and compositional inhomogeneities induced during straightening by hot plastic deformation, some regions acting as strong stress concentrators. In compression and bending stresses the mechanical behavior is not different, but the presence of stress concentrators influences the scattering of the results.

The corrosion test of some samples obtained from the metallic body elements subjected to experimental research required the completion with information through the surface properties. The conclusions of the experimental researches indicate a better corrosion behavior of the reconditioned metal body part by hot plastic deformation, using the "spotter" technique.

The investigation of the surface wettability by assessing the contact angle and determining the surface energy indicated that the metal elements of the body reconditioned by hot plastic deformation have different surface properties than the undeformed ones.

An innovative element proposed in this doctoral thesis was the attempt to improve the corrosion resistance of metal elements, after reconditioning them by hot plastic deformation, by coating them with alumina using thermal spray in plasma jet. The coating method can be implemented at the industrial level, and the experimental determinations of corrosion resistance testing revealed an improved behavior of the coated samples.

Following the correlation of all experimental results obtained in this doctoral thesis, it can be said that it is necessary to control the heating process of metal body elements when they are reconditioned by hot plastic deformation, so as not to induce microstructural changes that affect the properties mechanical.

Regarding the thermo-mechanical processing technologies used at industrial level, it is recommended to avoid heating with oxyacetylene flame of metal body parts in order to recondition them because it induces changes in the grain size of steels, thus affecting the mechanical properties of reconditioned parts. Induction or spotter heating ensures a controllable zone heating that does not induce major changes in microstructural characteristics, ensuring better mechanical properties for reconditioned parts.

Regarding the innovative potential of the doctoral thesis, it introduces the alumina coating using the thermal spray in plasma jet of the metallic elements of the car body after their reconditioning by thermo-mechanical methods.

Also, in the doctoral thesis it was shown that the mathematical models currently used by experts for the assessment of road accidents should include material aspects related to metal body elements, respectively microstructural aspects, history of thermo-mechanical processes suffered by them. elements during operation and mechanical properties.

C2. ORIGINAL CONTRIBUTIONS

The author highlights very clearly in this doctoral thesis a fundamental aspect of engineering and materials science, namely that the processing of metallic materials by thermo-mechanical methods induces microstructural and surface changes that influence the mechanical properties and surface properties of industrial parts made of materials. metallic.

The effect induced by the thermo-mechanical processing of the metallic elements of the car body during their reconditioning interventions has been quite little studied in the specialized literature, and this thesis comprehensively treats this subject both theoretically and practically. .
It should be noted that this doctoral thesis has a strong application at the industrial level, and the use in this thesis of an impressive number of experimental samples is due to the support provided by an industrial partner in the field of reconditioning of metal bodywork.

The author carried out a complex study on the processing of metal bodywork elements subject to road accidents and the methods of reconditioning metal bodywork elements used at industrial level. Not only the theoretical aspects were identified, but also the practical aspects regarding the procedures, work parameters and equipment currently used at industrial level, in order to be able to perform a comparative analysis and to offer solutions to streamline these activities at industrial level.

Another original contribution was the analysis of road accident assessment methods, both in terms of theoretical and practical assessment, as well as modern methods using reconstruction programs. An extremely important element has thus been identified, namely the fact that the reconditioning of metal car body elements is not taken into account when assessing road accidents.

This doctoral thesis proposes solutions for the optimal use of thermo-mechanical processing technologies for the reconditioning and commissioning of metal body elements that have been involved in road accidents that have resulted in deformations of these parts, ensuring a repeatability and reproducibility of results.

The complex way of investigating the mechanical behavior of experimental samples from car body metal parts in correlation with microstructural aspects can be considered an original contribution.

Studying the behavior of the specimen and suggesting a model for approximation, such as series springs, is a starting point in the mathematical description of the deformation process of an inhomogeneous structural material.

The establishment of a thermo-mechanical processing technology, respectively by hot plastic deformation with the zonal control of the heating that can be applied to avoid the uncontrolled increase of the grain size during the heating is an original contribution. The standardization of these procedures at the industrial level will lead to obtaining repeatable and reproducible results in terms of reconditioning the metal parts of the car body after they have been deformed as a result of collisions.

Carrying out a comparative study of the thermo-mechanical processing methods by hot plastic deformation applied at industrial level is also an own contribution of the author, thus

identifying the practical problems associated with each method and suggesting their remedy by establishing procedures. For work.

One can note the complex evaluation of the corrosion resistance of the experimental samples, which involved in addition to using the linear polarization technique by tracing the polarization curves by measuring the open circuit potential and tracing the linear polarization curves, and evaluating the sample surfaces following corrosion tests by stereomiscroscopy and scanning electron microscopy.

An own and original contribution of the author is the alumina coating of the metal parts of the car body after they have been reconditioned by thermo-mechanical methods, in order to improve the characteristics in operation. The author also not only performed a simple characterization of the submission, but also evaluated the efficiency of this coating from an industrial point of view.

Another original contribution is the introduction of experimental studies to determine the wettability of the surface. This is explained by the fact that metal body elements involved in road accidents and reconditioned by different techniques are to be applied to the surface, after this reconditioning, different putty or paint materials. The adhesion of these materials to the surface of reconditioned metal samples is influenced by the surface properties, respectively by the wettability of the surfaces.

As far as experimental research is concerned, they have been carried out under laboratory conditions which, to a large extent, reflect the operating conditions. Experimental research in this doctoral thesis can be extended by conducting experimental research at the industrial level, on reconditioned metal body elements and mounted on vehicles, but they can be carried out with the support of important companies in the automotive industry. This doctoral thesis has clearly highlighted the importance of experimental research and methods specific to the field of engineering and materials science for the automotive industry.

An extremely important element is the fact that in the present thesis it is demonstrated that the correct expertise of road accidents should include the material aspects related to metal body elements, respectively microstructural aspects, the history of thermo-mechanical processes suffered by these elements in operating time and mechanical properties.

The results of this doctoral thesis bring concrete elements in support of the introduction of material issues in road accident expertise, which can lead to a more concrete expertise of road accidents and which can have major social implications.

Last but not least, the author's contribution to the enrichment of the literature on the processing of metallic materials used in the automotive industry is another aspect that needs to be mentioned.

C3. VALUATION OF RESULTS

The results obtained in this paper were disseminated through 3 participations in national and international conferences, the publication of 5 scientific papers of which 5 indexed Clarivate Analytics.

Lucrări ştiinţifice publicate în reviste ISI WoS

1. **Navodariu N.**, Branzei M., Ciocoiu R., Ciuca I., Coman R., Raiciu A.D., Semenescu A., Antoniac I., Gradinaru S., Cristescu I., *Effect of local heating on the mechanical characteristics of repaired automotive panels*, Materiale Plastice, Volume 56, 2019, Pages 750-758. **IF 1,517**
2. **Navodariu N.**, Ciocoiu R., Coman R., Trante O., Raiciu A.D., Vasile M., Ciuca I., Cristescu I., *Corrosion behavior of welded repaires for water turbine blades*, Revista de Chimie, Volume 70, Issue 7, 2019, Pages 2497-2501. **IF 1,755**
3. **Navodariu N.**, Ciocoiu R., Dinita A., Trante O., Milea C., Ciuca I., Coman R., Saceleanu V., *Surface repairs by mmaw and mig-influences on fracture energy*, UPB Scientific Bulletin, Series B: Chemistry and Materials Science, Volume 81, Issue 3, 2019, Pages 209-218.
4. **Năvodariu N.**, Ghiban B., Rucai V., Săceleanu V., Bran D.-T., *The influence of the heat treatment over the mechanical behavior of steels used for alternator shafts*, UPB Scientific Bulletin, Series B: Chemistry and Materials Science, Volume 81, Issue 3, 2019, Pages 219-231.
5. **Năvodariu, N.,** Antoniac, I. Tăbăraș, D., Grigorescu, G., Ciocoiu, R., Trante, O., Turcu, R., Necșulescu, A., Raiciu, A.D., A study on the mechanical properties of car panels straightened by four methods, UPB Scientific Bulletin, Series B: Chemistry and Materials Science, Volume 82, Issue 4, 2020, Pages 257-272

Lucrări ştiinţifice publicate în reviste indexate în alte baze de date (Scopus, Google Scholar)

1. **Navodariu N.**, Antoniac I., Ciocoiu R., Trante O., Bololoi R., Tabaras D., Cernea A., Gradinaru S., *A study on surface wetting and corrosion behavior of straightened car panels*, Revista de Chimie, Volume 71, Issue 4, 1 April 2020, Pages 267-276.
2. **Navodariu, N.,** Ciocoiu, R., Trante, O., Antoniac, V. I.. *Materials for Automotive Industry and their Influence on the Dynamics of a Car Crash*, Journal of Engineering Studies and Research, 25(2), (2019), 25-32.

Lucrări prezentate la conferințe internaționale

1. **Navodariu N.**, Antoniac I.V., Ciocoiu R., Trante O., "*Materials for automotive industry and their influence on the dynamics of a car crash",* 7th International Conference on Materials Science and Technologies, *RoMat' 2018,* 15-18 November, Bucharest, Romania.
2. **Navodariu N.,** Antoniac I.V., Ciocoiu R., Trante O., Bololoi R., Tabaras D., Cernea A., Gradinaru S., *A study on surface wetting and corrosion behavior of straightened car panels,* International Conference organised by "VASILE ALECSANDRI" University of Bacau – Faculty of Engineering, 22-24 May 2019, Bacau, Romania.
3. **Navodariu N.**, Ciocoiu R., Dinita A., Trante O., Milea C., Ciuca I., Coman R., Saceleanu V., *Surface repairs by mmaw and mig-influences on fracture energy*, 1st International Conference on Medical Materials Science & Engineering, *1Biomat*, 20-23 February 2020, Predeal, Romania.

SELECTIVE BIBLIOGRAPHY

[1] A. Hambali, S.M. Sapuan, N. Ismail, Y. Nukman, Material selection of polymeric composite automotive bumper beam using analytical hierarchy process, Journal of Central South University of Technology, vol. 17, pp. 244–256, 2010.

[2] M.P. Todor, I. Kiss, Systematic approach on materials selection in the automotive industry for making vehicles lighter, safer and more fuel efficient, Applied Engineering Letters, vol. 1, pp. 91-97, 2016.

[3] G. Minciună, P. Vizureanu, D. C. Achiței, A. V. Sandu, A. Berbecaru, I. G. Sandu, Structural characterization and properties analysis of CoCrMoSi Alloys, Journal of Optoelectronics and Advanced Materials, vol. 18, pp. 174-178, 2016.

[4] D.P. Burduhos-Nergis, P. Vizureanu, A.V. Sandu, C. Bejinariu, Evaluation of the Corrosion Resistance of Phosphate Coatings Deposited on the Surface of the Carbon Steel Used for Carabiners Manufacturing, Applied Sciences, vol. 10, 2020.

[5] E. Ghassemieh, Chapter: Materials in Automotive Application, State of the Art and Prospects, book: New Trends and Developments in Automotive Industry, Ed. InTech, pp. 365-394, 2011.

[6] M. Nicoara, C. Locovei, V. A. Șerban, R. Parthiban, M. Calin, M. Stoica, New Cu-Free Ti-Based Composites with Residual Amorphous Matrix, Materials, vol. 9, pp. 331, 2016.

[7] R. Rana, S.B. Singh, Automotive Steels: Design, Metallurgy, Processing and Applications, Woodhead Publishing, ISBN: 978-0081006382, 2016.

[8] R.Y. Fu, X.C. Wei, W. Shi, L. Li, B. De Cooman, P. Wollants, X.D. Zhu, L. Wang, Dynamic tensile characteristic of high strength low alloy TRIP steel and its modelling, Proc. International Conference on TRIP-Aided High Strength Ferrous Alloys, GRIPS, pp. 287-291, 2002.

[9] R. Kuziak, R. Kawalla, S. Waengler, Advanced high strength steels for automotive industry: a review, Archives of Civil and Mechanical Engineering vol. 8, pp. 103-117, 2008.

[10] Plastics and Polymer Composites Technology Roadmap for Automotive Markets, Plastics Division of the American Chemistry Council, 2014.

[11] Aalco - Ferrous and Non-Ferrous Metals Stockist, Aluminium: Specifications, Properties, Classifications and Classes, 2005.

[12] M. Wilhelm, Materials used in automobile manufacture – current state and perspectives, Journal de Physique IV Proceedings, EDP Sciences, 1993.

[13] S. Jayasathyakawin, M. Ravichandran, N. Baskar, C. Anand Chairman, R. Balasundaram, Mechanical properties and applications of Magnesium alloy – Review, Materials Today: Proceedings, vol. 27, pp. 909-913, 2020.

[14] M. Shib, Material selection and design, University of Illinois at Urbana-Champaign (UIUC), 2007.

[15] W.S. Miller, L. Zhuang, J. Bottema, A.J. Wittebrood, P. De Smet, A. Haszler, A. Vieregge, Recent development in aluminium alloys for the automotive industry, Materials Science and Engineering: A, vol. 280, pp. 37-49, 2000.

[16] M.K. Kulekci, Magnesium and its alloys applications in automotive industry, The International Journal of Advanced Manufacturing Technology, vol. 39, pp. 851–865, 2008.

[17] P. Patil, Applications of composite materials in the automobile industry, Advanced material technology, 2009.

[18] A.Panda, K.Dyadyura, Polymer composites for automotive sustainability, European technology platform for sustainable chemistry, ISBN: 978-3-942303-84-2, 2018.

[19] Deborah D.L. Chung, Carbon Fiber Composites, Chapter 4, Properties of Carbon Fibers, Butterworth-Heinemann, ISBN 978-0-08-050073-7, 1994.

[20] Trzaska, J. et al., Modelling of CCT Diagrams for Engineering and Constructional Steels, Journal of Materials Processing Technology, pp. 504-510, 2007.
[21] L.R. Cucuruz, M. Nicoară, Elaborarea și solidificarea materialelor, Editura: Politehnica, Timisoara, Seria: Stiinta materialelor, ISBN: 978-606-554-751-3, 2013.
[22] S. J. Lee et al., Prediction of austenite grain growth during austenitization of low alloy steels, Materials and Design, 29, 1840-1844, 2008.
[23] L.A. Girifalco, R.J. Good, A theory for the estimation of surface and interfacial energies I. Derivation and application to interfacial tension, The Journal of Physical Chemistry A, vol. 61, pp. 904-909, 1957.
[24] H.K.D.H Bhadeshia, Bainite in Steels, 2nd ed., The Institute of Materials, London, 2001.
[25] G.B. Olson and W.S. Owen, Martensite – A Tribute to Morris Cohen, , Eds., ASM International Materials Park, OH, 1992.
[26] Cullison A., Engineer Provides Flame Straightening Techniques, Welding Journal, vol. 74, 1995.
[27] Vackar B. K., Dolida, R. J., Effect of Flame Straightening Heat on Austenitic Stainless-Steel. Welding Journal, vol. 60, pp. 25-27, 1981.
[28] J. Argen, On the classification of phase transformations, Scripta Materilia, vol. 46, pp. 893-898, 2002.
[29] H.K.D.H. Bhadesia, Worked Examples in the Geometry of Crystals, The Institute of Materials, London, 1987.
[30] J.W. Christian, The Theory of Transformations in Metals and Alloys, 2nd ed., Part 1, Pergamon Press, Oxford, 1981.
[31] H.I. Aaronson, Decomposition of Austenite by Diffusional Processes, Interscience, New York, 1962.
[32] M.C. Perju, P Vizureanu, Chemical compounds analysis developed on the micro alloying area of coating layers obtained by impulse discharge method, Revista de Chimie, vol. 65, pp. 694-696, 2017.
[33] Zhao D. S., Huang Z. Y., Miao T. J., Experimental Parameter Calculation of Welding Deformation Correction by Flame Straightening, Destech Trans Mat, pp. 33-38, 2016.
[34] Lacalle R., Alvarez J. A., Ferreno D., Portilla J., Ruiz E., Arroyo B., Gutierrez-Solana F., Influence of the Flame Straightening Process on Microstructural, Mechanical and Fracture Properties of S235 JR, S460 ML and S690 QL Structural Steels, Exp Mech, vol. 53, pp. 893-909, 2013.
[35] N. Navodariu; M. Branzei; R. Ciocoiu; I. Ciuca; R. Coman; R. A. Daniela; A. Semenescu; I. V. Antoniac; S. Gradinaru; I. Cristescu: Effect of local heating on the mechanical characteristics of repaired automotive panels, Materiale Plastice, 2019.
[36] A. Gnatov, S. Argun, New method of car body panel external straightening: tools of method, International Journal of Vehicular Technology, 2015.
[37] Gh. Frăţilă, Gh. Mărculescu, Sistemele de frânare ale autovehiculelor, Editua Tehnică, Bucureşti, 1986.
[38] V. Panáček, M. Semela, V. Adamec, B.Schüllerová, Impact of Usable Coefficient Of Adhesion Between Tyre and Road Surface by Modern Vehicle on Its Dynamics While Driving and Braking in the Curve, Transport, vol. 31, pp. 142–146, 2016.
[39] B. Pałasz, K.J. Waluś, Ł. Warguła The determination of the rolling resistance coefficient of a passenger vehicle with the use of selected road tests methods, MATEC Web of Conferences, vol. 254, 2019.